Protracted Colored Noise Dynamics Applied to Nanoscale Studies of Block Copolymers

A Dissertation
Presented to
The Academic Faculty

by

Daniel L Nicoloso

In Partial Fulfillment
of the Requirements for the Degree
Chemical Engineering with Research Option in the
School of Chemical and Biomolecular Engineer

Georgia Institute of Technology
May 2015

Protracted Colored Noise Dynamics Applied to Molecular Dynamics of Block Copolymer

Approved by:

Dr. Clifford Henderson, Advisor
School of Chemical and Biomolecular Engineering
Georgia Institute of Technology

Dr. Peter Ludovice
School of Chemical and Biomolecular Engineering
Georgia Institute of Technology

Andrew Peters
School of Chemical and Biomolecular Engineering
Georgia Institute of Technology
Date Approved:

Protracted Colored Noise Dynamics Applied to Molecular Dynamics of Block Copolymer

Approved by:

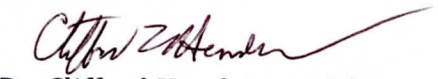

Dr. Clifford Henderson, Advisor
School of Chemical and Biomolecular Engineering
Georgia Institute of Technology

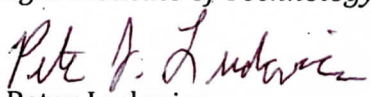

Dr. Peter Ludovice
School of Chemical and Biomolecular Engineering
Georgia Institute of Technology

Andrew Peters
School of Chemical and Biomolecular Engineering
Georgia Institute of Technology
Date Approved: 4/30/15

ACKNOWLEDGEMENTS

I would like to thank my advisor Dr. Clifford Henderson for providing the opportunity to work on this project. I would also like to thank Andrew Peters for his assistance and for allowing me to work on a project that he was leading. I acknowledge all the other members of the Henderson Research group for timely assistance along the way. I would like to thank Air Products for funding this opportunity. Finally, a special thanks to Dr. David Sherrill. It was your Physical Chemistry II course that inspired me to take part in this research.

TABLE OF CONTENTS

LIST OF TABLES

LIST OF FIGURES

Abstract

Coarse-grained molecular dynamics is an accurate and versatile tool for understanding the dynamic behavior of molecules at a wide variety of length and time scales. This especially useful for understanding the kinetics of self-assembly processes in block copolymers, as these systems are difficult and expensive to study experimentally. One of the current limitations of molecular dynamics simulations is that when molecules in the system must overcome a large activation energy barrier, the computing speed decreases by several orders of magnitude. Protracted colored noise dynamics is a variation of molecular dynamics, which was developed to address the issue by incorporating stochastic colored noise into force calculations in simulation. Hypothetically, this should improve phase space sampling efficiency in molecular dynamics simulations and force kinetically inhibited systems to an equilibrium state more quickly. The purpose of this study was to apply protracted colored noise dynamics to simulations of block copolymers, including systems with kinetic limitations. The first goal of this study was to investigate potential computational speed up due to overcoming kinetic limitations with protracted colored noise dynamics. The results were very promising, showing an order of magnitude reduction in computational time for high activation energy simulations. The second goal was investigate the effect of random forces on the equilibrium structure of block copolymers in simulation. The results show that for sufficiently strong random forces, the block copolymers are highly disordered at equilibrium. In the course of this study, a threshold parameter space for protracted colored noise dynamics was developed to understand the limitations on noise strength.

Chapter 1: Introduction

Coarse grained Molecular Dynamics (MD) is a computational technique that uses Newton's Second Law to model molecular systems. Movements of molecular aggregates are approximated as the motion of hard beads within a potential field. The negative gradient of the potential field (U(r)) is the force (F) acting on a bead. The acceleration (a) is the force divided by mass (m), and the acceleration can be integrated over time to determine the displacement (r) of a bead. For a given system, there can be many beads, and the potential field for each bead is determined by the interactions with every other bead in the system. Because all bead positions change over time, U(r) will also change over time, making the problem highly complex. In general, this problem must be solved numerically by assuming that acceleration is constant over a very small time step and then integrating over discrete

$$F_i = -\nabla U(r_i) = m * a_i \quad (1)$$

$$v_{i+1} = a_i * \Delta t + v_i \quad (2)$$

$$r_{i+1} = 0.5 * a_i * \Delta t^2 + v_i * \Delta t + r_i \quad (3)$$

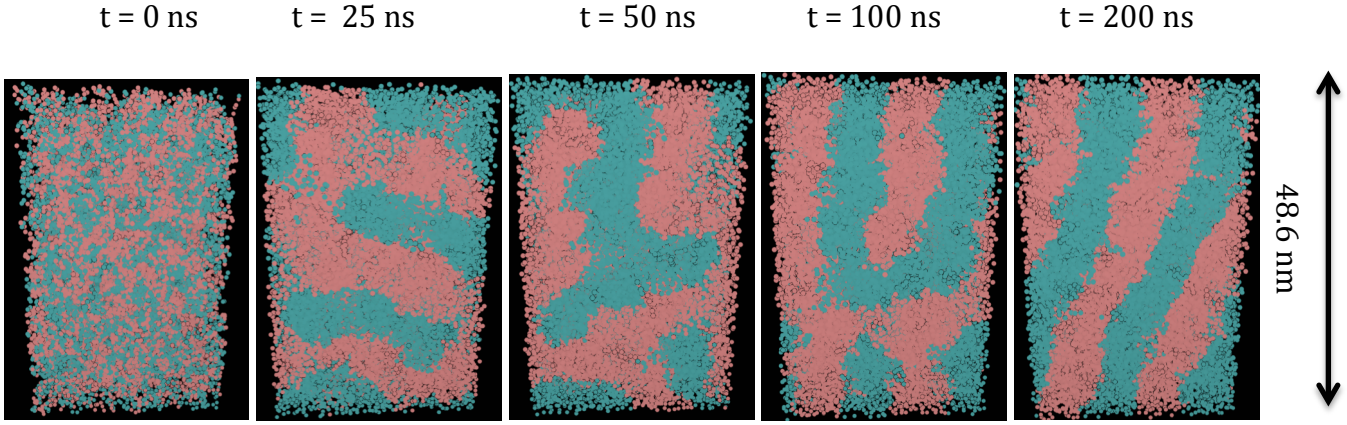

Figure 1: Dynamic Phase Separation of Block Copolymers Demonstrated in Simulation

time steps. The basic iterative scheme is described in Equations 1-3, using Newton's equations of motion to calculate velocity (v_i) and displacement (r_i) during constant acceleration. By using this scheme, the time dependent behavior of the beads can be found. This is advantageous for modeling molecular systems because it reveals dynamic and equilibrium behavior, as opposed to mean field techniques, which only solve for the equilibrium behavior.[1]

The relevant application considered in this study is the modeling of directed self-assembly (DSA) of block copolymers (BCPs). BCPs are chains consisting of two or more different monomers. The monomers have different properties and tend to form separate phases at equilibrium. The phase separation occurs over nanoseconds, as is seen in the simulated BCPs in Figure 1. By controlling the phase separation, the BCPs can be used to form nanoscale patterns in optical lithography, which is used in the production of integrated circuits. DSA is a new technique that uses BCPs for imprinting lithographic patterns on the scale of tens of nanometers.[1] This could lead to development of smaller integrated circuits, which would lead to more powerful electronic devices. However, experiments on BCPs are expensive and difficult to analyze, which necessitates the use of computer models to understand their behavior. Coarse grained MD has great potential for this application because of realistic polymer interactions, and the ability to study the kinetics of DSA processes.[1]

Atomistic MD is an alternative that has been used to study BCPs. Atomistic MD does not use coarse graining, so it produces details at the level of atoms, as opposed to the hard beads used in coarse grained MD. Although this yields a much higher level of detail, the computational time required restricts the use of these models to relatively small systems over very short time scales.[2] If this was used to model a DSA process, weeks would be required to

complete a single simulation. Previous research has developed an effective coarse graining algorithm for simulations of BCP systems, which aggregates the properties of several monomers to those of a single bead.[1] This leads to simulation run times that are orders of magnitude shorter than those of comparable atomistic simulations.[1]

The most commonly used alternative to coarse grained MD is mean field theory, which uses a thermodynamic free energy function. The equilibrium state of the system can be found by minimizing the free energy function.[2] It is useful because of high speed, but it fails to capture phase change kinetics, which are relevant to the study of DSA for BCPs. Prior research has found that through parallel computing and coarse graining, MD can reach computational speeds similar to mean field.[1]

However, MD simulations still run into problems when high-energy defects occur in the simulation. An example would be a BCP system with a broken lamellae, which requires the simulation to overcome a large activation energy. This causes an exponential increase in real time computing because of slower kinetics. The purpose of this study was to apply protracted colored noise dynamics (PCND) to simulations of BCPs. PCND adds stochastic colored noise to conventional MD force calculations. The random forces increase the phase space sampling efficiency of the simulation.[5] This means that it can overcome a large activation energy barrier by broadening the energy distribution. This reduces the time necessary for the simulation to reach equilibrium and so reduces the necessary real time computing. The problem with this is that the simulation may overcome energy barriers that were never intended and result in equilibrium states that deviate from the normal behavior of the model. In extreme cases, this results in physically inaccurate states.

In this research, the PCND method was applied to coarse grained simulations of BCPs with two different initial states: mixed and high energy defective. The final state of each simulation type was lamellar phase separated. The simulations were run on specialized GPUs because of the need for parallel computing. The results of the mixed state simulations were used to characterize perturbations from normal behavior due to PCND and to determine the limitations on PCND parameters. Even though mixed state simulations have very reasonable run times, it was necessary to apply PCND to these simulations to compare the results with conventional MD. The defective state simulations were used to test whether PCND could reduce real time computing. The results suggest that PCND can move these kinetically inhibited simulations to equilibrium orders of magnitude faster than would otherwise have be possible. By fine-tuning the PCND parameters, this can be accomplished with a minimal loss of accuracy. PCND is a very effective way to improve MD computational speed. This has been shown for defective BCP simulations, but it could have broader applications to other higher complexity molecular systems with high activation energy barriers.

Chapter 2: Literature Review

Molecular Simulation

Molecular dynamics (MD) is a technique that models the motion of molecular systems using Newton's Second law. It is advantageous because of high accuracy and because of the ability to study the kinetics of molecular behavior.[1] These factors are critical to the simulation of many processes, but they come at the expense of computational speed. In this research, directed self-assembly (DSA) of block copolymers (BCPs) is modeled, which is relevant to the optical lithography used in the production of semi-conductors. An effective simulation of DSA must reflect the kinetics of BCP phase separation,[1] which is why the development of high speed MD is critical. Previous work has shown that coarse graining and parallel computing can improve speed for these simulations.[1] However, when the simulation must overcome a high activation energy barrier, the computational time is still unreasonably long.

The most commonly used alternative to MD is Mean Field Theory. This method solves for thermodynamic properties by minimizing the free energy function.[2] The advantage of this is high computational speed, but it only determines the equilibrium state of the system. Xu and Zhang demonstrate a variation of mean field theory called Self-Consistent Field Theory (SCFT), and show how it can be used to simulate confined systems of BCPs.[3] Another alternative approach is Monte-Carlo simulations. These simulations solve for thermodynamic properties by using a random sampling of the possible states of the molecular system. The average properties of all sampled states is used to evaluate the equilibrium state of the system.[4] Though both methods can be used to study block copolymer systems, they cannot access the dynamic behavior of the system, which is necessary for modeling DSA.

Protracted Colored Noise Dynamics

Jenkins explored a possible solution to the problem of high activation energy MD simulations. He proposed and tested a solution called protracted colored noise dynamics (PCND). This algorithm applies stochastic forces (ε(t)) to the beads in MD simulations, as

$$F_i = -\nabla U(r_i) + \varepsilon(t_i) \qquad (4)$$

$$\frac{d\varepsilon(t)}{dt} = \frac{\eta(t) * \Omega^{0.5} - \varepsilon(t)}{\tau} \qquad (5)$$

shown in Equation 4. The distribution of forces is exponentially correlated over time, as opposed to a Gaussian white noise distribution. PCND gives the simulation better phase space sampling efficiency which allows it to overcome energetic barriers.[5] The correlated distribution of forces is defined by the stochastic differential equation Equation 5, where η(t) is a Gaussian distribution.[5] The mean of ε(t) is 0, but the correlation over time is a decaying exponential. There are two significant parameters that define the distribution of random forces. The first is Ω/τ, which is the root mean squared random force. This affects the intensity of the random forces. The second parameter, τ, is the decay constant of exponential correlation over time. The exponential correlation is similar to typical molecular phyiscs.[5]

A study by Jenkins applied PCND to the simulation of a single particle in a bistable potential.[5] A bistable potential has two equilibrium states, separated by an energy barrier, as shown by the function in Figure 2. The average time necessary for the particle to pass over the energy barrier (Mean First Pass Time or MFPT) was measured for a wide variety of Ω/τ and τ. The results suggested that increasing either variable would increase the noise intensity of the simulation, and as a result, reduce the MFPT.[5] More interesting is the fact that for constant Ω/τ there existed local minimum of MFPT as a function of τ.[5] The implication of

this research is that PCND can improve computational time when significant energy barriers must be overcome, and that there is an optimal noise intensity that will achieve fastest equilibration speed for a given system. Further, the results of the bistable potential simulations were confirmed by an earlier experimental result with an electronic circuit.[5] Hanggi and his colleagues studied it using a noise generating filter in combination with an integrating circuit element.[5] The parameters on the noise generating filter were analogous to Ω/τ and τ in PCND. The results suggested that increasing colored noise intensity would reduce the mean sojourn time, which is the time necessary for the circuit to transition from one steady state voltage to another (analogous to MFPT).[6] The studies on these simple systems suggest that the application of colored noise could reduce equilibration time for a broad range of non-linear systems, not just MD simulations.

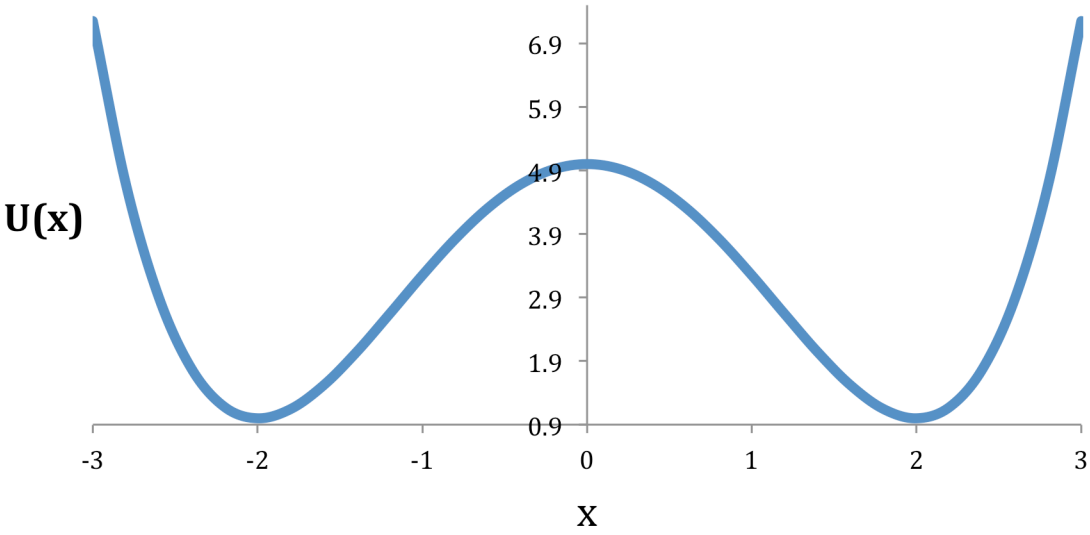

Figure 2: Bistable Potential Function

Jenkins also applied the algorithm to the simulation of a Lennard-Jones (LJ) glass: a simple simulation where each bead has only un-bonded interactions with the others.[5] The model in this study had 1000 particles,[5] which means that it was far more complex than the

bistable potential simulation discussed above. It was found that with appropriate PCND parameters, the simulation reached equilibrium about 3000 times faster.[5] However, it was noted that some PCND parameters lead to systems that failed to equilibrate normally.[5] This leads to a conclusion that PCND parameters must be selected carefully or else the system will be perturbed from its normal equilibrium state, at which point, the MD simulation loses significant accuracy.

The goal of this study was to apply the PCND method to systems of BCPs in DSA. Jenkins applied the technique to two systems that were very simple. Additional complexities are introduced in a BCP system. First, since the beads used in this research represent polymers, they have bonded potentials, where previous work only addressed beads existing in non-bonded potentials. The second distinction is that BCPs consist of two different types of beads, A and B types. This means that there are several non-bonded potentials to consider: the interaction of A-A, B-B, and A-B. This is more complex than the LJ glass, which only used a single type of bead, and a single type of non-bonded interaction. Finally, in this research, random forces are directed along the contour of the polymer, whereas Jenkins used randomly directed forces. This research extends the PCND method simulations of block copolymers to see if computational time can be reduced by this technique.

Block Copolymers

Block copolymers are polymers that consist of two or more different monomers. These monomers have a tendency to phase separate on the scale of nanometers.[7] They have received significant attention because of the ability to form small patterns in the fabrication of devices,[7] especially electronics. In general, these polymers exhibit a single pattern

morphology (e.g. lamallae, cylinders) in a thin film.[7] In such a thin film, the size of the microphase domain size can be controlled by the molecular weight of the polymers.[8] The microphase separation is a diffusive process and as the molecular weight of the polymer chains increases, the process becomes slower. At sufficiently large molecular weights, the chains may end up trapped in a non-equilibrium, poorly ordered state.[8] Xu and his co-authors found that by controlling molecular weight of copolymers, they could achieve cylindrical phases with diameters of 14 – 50 nm.[8] This is relevant to the work in the present study, because we are endeavoring to simulate block copolymers in thin films, and chain length is a relevant parameter to consider.

Applications in lithography benefit from having a smoother interphase between the two microphases. It is important to quantify the roughness of the interphase for this purpose. Zhao and his co-authors quantified roughness using a metric called Line Edge Roughness (LER). This is defined as three times the standard deviation of the phase interphase edge location relative to a reference.[9] This metric was minimized to develop good patterning in stochastic simulations. This is not the method that will be used to quantify roughness in this paper, but the concept is useful for understanding what is meant when roughness is discussed.

In monodisperse polymer mixtures, the movement of polymer chains in an entanglement is primarily due to reptation.[10,11] A polymer chain is surrounded by a tube that is made of all the adjacent polymers. Reptation refers to the movement along the tube. Events besides reptation can still occur, such as tube renewal or tube dilation,[11] but experiments have confirmed that a purely reptational model is accurate for monodisperse mixtures at high molecular weights.[11] Because the simulations in this research are inherently monodisperse,

the forces used in this variation of PCND are only directed along the contour of the chain, which will drive reptation. Because reptation is the primary means of motion, this is expected to produce more useful diffusive motion.

The driving force for phase separation of block copolymers is a reduction in potential energy (U). For diblock copolymers, this reduction comes from the fact that the unbonded interaction between A monomers and the B monomers has less potential energy than the same monomer interactions. The phase separation occurs in order to maximize A-B interactions and minimize A-A and B-B interactions. In simulation, these interactions come the Lennard-Jones equation, which represents van der waals interactions.[1] χ (Flory-Huggins Interaction Parameter) is a property that represents resistance to phase separation. It is frequently measured in experimental and mean field studies.[1]

X-ray Scattering

X-ray scattering is technique that measures the intensity of an electric field generated by elastic electron scattering of particles in the sample.[12] The intensity I(q) is the square of the magnitude of the electric field (E).[12] E is related to the electron density ($\rho(r)$) by a fourier transform:

$$E = A \int \rho(r) e^{-i*q*r} \, dr \qquad 6$$

, where A is a constant, q is wavelength, and r is the distance along a radial dimension.[12] This is frequently used to analyze the structural characteristics of polymers. There are two categories of scattering: small angle x-ray scattering (SAXS) and wide angle x-ray scattering (WAXS).[13] When applied to polymeric materials, the former can be used to characterize

crystalline lamellae at the level of nanometers,[13] which makes it more relevant to the research discussed in this paper.

The SAXS pattern can be used to characterize several relevant morphological features. The most significant would be the presence of ordered structural formation in block copolymer lamellae. Normally, block copolymers will form straight lamellae, but applying random forces could induce disordered (or heavily curved) pattern. This makes the ordering random and could produce a broadening of the scattering peaks.[14] In scattering literature, this trend would be called "liquid scattering".[14] Observing liquid scattering may provide a useful criterion of performance for PCND simulations relative to non-PCND.

Chapter 3: Materials and Methods

General

All BCP simulations were scripted in HOOMD (Highly Optimized Object Oriented Molecular Dynamics), a particle simulation toolbox developed in Python. It was developed as part of a collaborative effort lead by the Glotzer research group at University of Michigan. MD simulations were run on Intel Dual Core Processors with accelerated GPUs for highly parallelized computing. A variation of the script used to set up the simulations is included in Appendix A. Visual Molecular Dynamics (VMD) was used for visualizing the results of the simulations and performing certain calculations. VMD was developed by the Theoretical and Computational Biophysics group at the University of Illinois at Urbana-Champaign. MATLAB and Microsoft Excel were also used extensively for data analysis and visualization.

The studies conducted fall into two categories: mixed state and defective state block copolymers. These two types used the same HOOMD script but differed in the initial conditions and different criterion that were analyzed. The mixed state studies were primarily intended to study morphological effects of PCND, and the defective state studies were primarily intended to study the speed up from using PCND. In both cases, the positions and properties of the particles were specified within a box with periodic boundary conditions. All simulations were run with linear chains that consisted of a single section of A beads connected to a single section of B beads. The fraction of A beads (f_A) was kept at 0.50 for all simulations. Coarse graining was such that each bead represented 4 monomers.

Three kinds of interactions were used in these simulations. The first was a stretching interaction, which reflected the potential energy of a bond between two beads, as shown in Equation 7:

$$U_{str}(r) = k_{str}(r - r_{eq})^2 \quad (7)$$

, where r refers to the bond length, r_{eq} is the equilibrium bond length, and k_{str} is the stretching constant. Every pair of bonds forms an angle, and the second interaction type is bond angle interactions. Every bond angle has a relevant harmonic as described by Equation 8:

$$U_{ang}(a) = k_{ang}(a - a_{eq})^2 \quad (8)$$

, where a is the bond angle, a_{eq} is the equilibrium bond angle, and k_{ang} is the angular stretch constant. Note that this has a similar form to Equation 7, except that it is a function of angle not of bond length. All the constants for these two interactions were kept identical for each simulation. Non-bonded interactions were represented as a Lennard-Jones interaction as shown in Equation 9:

$$U_{ji}(r) = \varepsilon_{ji} * \left(\left(\frac{\sigma_{ji}}{r}\right)^m - \left(\frac{\sigma_{ji}}{r}\right)^{0.5m}\right) \quad (9)$$

, r is the distance between interacting particles, i and j are the particle types respectively, ε_{ij} is the proportional interaction constant, and σ_{ij} is the radial distance between particles where $U_{ij} = 0$ (equilibrium), and m = 8 for the purposes of this study. It should be noted that the LJ interactions between similar beads (A-A and B-B) was kept identical at 0.5 kcal/mol, so the beads have identical same monomer interactions. The only parameter that was varied throughout was ε_{ab}, the unbonded interaction constant between A and B types. Table 1 shows all the above constants and the values that were used.

Table 1: Interaction Constants used in Simulations

Symbol	Interaction	Value
k_{strA-A}	A-A (bond)	100 kcal/mol-nm^2
k_{strB-B}	B-B (bond)	100 kcal/mol-nm^2
$k_{angA-A-A}$	A-A-A (angle)	5 kcal/mol
$k_{angB-B-B}$	B-B-B (angle)	5 kcal/mol
r_{eqA-A}	A-A (bond)	0.82 nm
r_{eqB-B}	B-B (bond)	0.82 nm
$a_{eqA-A-A}$	A-A-A (angle)	$2\pi/3$ rad
$a_{eqB-B-B}$	B-B-B (angle)	$2\pi/3$ rad
σ_{A-A}	A-A (unbonded)	1.26 nm
σ_{B-B}	B-B (unbonded)	1.26 nm
σ_{A-B}	A-B (unbonded)	1.26 nm
ε_{A-A}	A-A (unbonded)	0.5 kcal/mol
ε_{B-B}	B-B (unbonded)	0.5 kcal/mol
ε_{A-B}	A-B (unbonded)	0.3 – 0.4 kcal/mol

Mixed State Studies

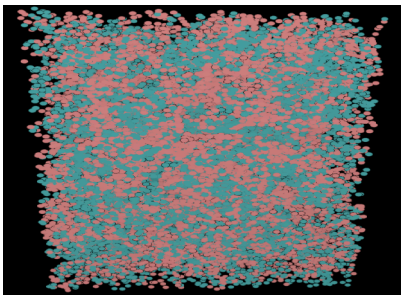

Figure 3: Mixed State Initial Conditions

The initial conditions for each simulation were block copolymers in a randomly mixed state. The purpose behind this was to study the effect of PCND on equilibrium morphology of the block copolymers in simulation. Because this system does not suffer from

kinetic limitations, it was possible to observe equilibrium behavior of both PCND and non-PCND simulations without requiring unreasonable real time computing. Different initial conditions were generated for three chain lengths in order to observe the effect of chain length on PCND results.

The only differences between initial conditions were the dimensions of the simulation box and the bead density. The dimensions of the box had to be varied in order to allow polymers of different chain length to behave naturally within the boundaries. It was observed that the box dimensions influenced morphological features of the polymers at equilibrium, and this was undesirable for observing the effect of chain length. The bead density refers to the number of beads per unit volume, and this was varied with the intent to keep the number of particles in each simulation approximately constant. Table 1 lists the dimensions and bead density of each box that was used as the initial conditions for the mixed state simulations. χ, the Flory-Huggins interaction parameter, was kept at 0.85 for all simulations.

Table 2: Initial Conditions for Mixed State Simulations

	Chain Length (beads)	Dimensions (nm^3)	Bead Density beads/nm^3	Number of Chains
Box 1	16	36.3x36.3x36.3	1.4	4185
Box 2	24	48.6x31.37x31.37	1.4	2790
Box 3	32	60.75x27.17x27.17	1.5	2093

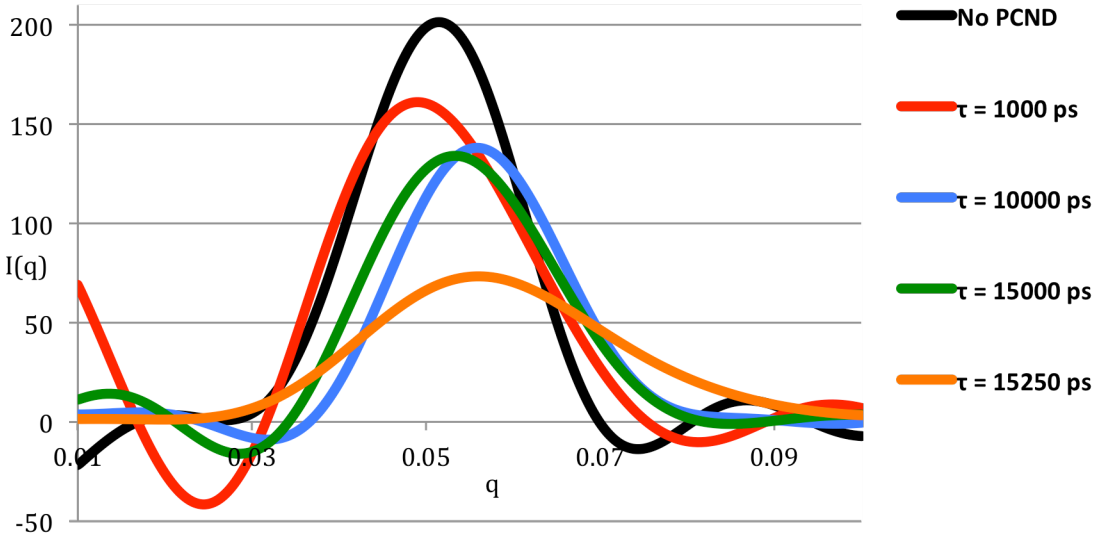

Figure 4a: X-ray Scattering Pattern Decay For Increasing PCND Noise at Ω/τ = 0.1 kcal/nm

Two morphologically relevant properties were calculated for the mixed state simulation results. These were both based on simulated electron scattering patterns of the block copolymers at equilibrium. To calculate these patterns, a radial pair distribution function was computed and this was converted to a scattering intensity pattern via a Fourier transform, as shown in Equation 6. Radial pair distributions were calculated using VMD. The first relevant morphological characteristic of the mixed state simulation results was the pitch of the block copolymers. The pitch was calculated along the direction perpendicular to the sides of the simulation boxes. Since many lamellae were tilted relative to the sides of the box, this makes it possible that the pitch measured for each simulation will deviate from the true pitch of the lamellae.

$$D = \frac{2\pi}{((1 + Er) * q_{max})} \qquad (10)$$

$$Er = 0.19054 * \left(\frac{2\pi}{(q_{max} * R_{max})}\right)^{2.4676} \qquad (11)$$

The calculation of pitch (D) was done with Equation 10, where q_{max} is the wavelength of the scattering vector that had the maximum intensity in the x-ray scattering. Er is an empirical corrective factor that can be computed from Equation 11, where R_{max} is the maximum distance between particles in the radial pair distribution calculation. Equation 11 is a correction that is needed because the integration of Equation 6 in this case is only to R_{max}, but in a real x-ray scattering it would be to infinity, and Er = 0. The correction is based on previous simulations with known pitches.

The second major property related to morphology was maximum scattering intensity (I_{max}) for each x-ray scattering pattern. This was collected for each mixed state simulation because it had an empirical relation with the formation of lamellae. It was found that for increasing PCND noise, the BCP lamellae became rougher at equilibrium. For sufficiently strong noise, lamellae completely failed to form at equilibrium, as shown in Figure 4b for polymers at a chain length of 16 beads.

This failure to form lamellae was characterized by a significant drop in the I_{max} of the x-ray scattering, and a general broadening of the scattering peaks, as shown in Figure 4a.

No PCND τ = 1000 ps τ = 10000 ps τ = 15000 ps τ = 15250 ps

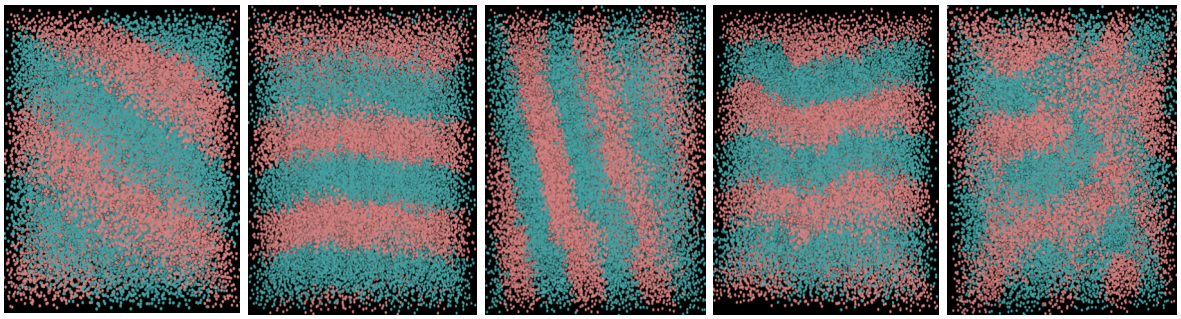

Figure 4b: Equilibrium Behavior For Increasing Noise Strength at Ω/τ = 0.1 kcal/nm

This agrees with x-ray scattering literature, which associates broader peaks with increased disorder. The drop in I_{max} relative to the non-PCND values was found to be the simplest metric to say whether lamellae had formed. It was generally found that simulations failed to form lamellae at I_{max} that were 50% of the non-PCND value. This is a coarse metric so it is possible that their could be lamellae below or near that criterion, but most results below that metric failed to form full lamellae. Furthermore, regardless of how close they were too the metric, lamellae had greater roughness for lower values of I_{max}. Since the goal of this metric was to characterize the useful PCND parameters, and smoother lamellae were more desirable for research, it was deemed that a coarse metric would be sufficient. The threshold parameters were determined to be the largest parameters that produced I_{max} below the criterion.

The equilibrium time step for each mixed state simulation was also collected. This was the time necessary for the spatially averaged potential energy (U(n)) of the system to reach steady state. Time was measured in discrete time steps (n), with a simulated time of

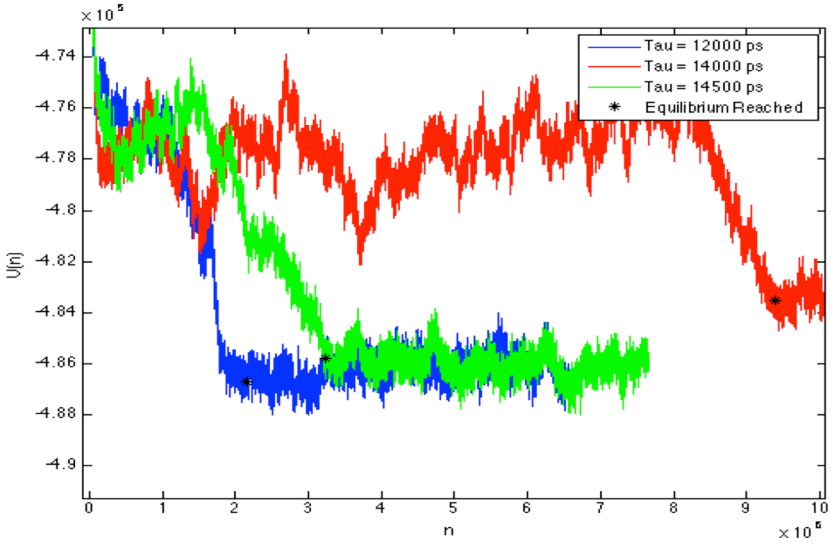

Figure 5: Examples of Potential Energy Over Time Curves for Ω/τ = 0.1 kcal/nm

0.05 ps between each discrete sample. Because of high frequency fluctuations, a single equilibrium potential energy had to be found by a averaging over the timesteps at the end of the simulation. The time average U(n) varied with the selection of the number of timesteps to average over, so an algorithm was developed to select the appropriate number of time steps (h) to average over. The initial guess was h = 10 timesteps, and the algorithm iteratively increased the number of timesteps by 10 until the average U(n) converged within 1000 kcal/mol. The potential energy signal was then filtered through a hundred point running average filter, and the equilibrium time step occurred was when the filtered potential energy signal passed through the average potential energy. Figure 5 shows three examples of potential energy curves, with the equilibrium potential energies and times shown in black dots.

For each combination of Ω/τ and τ, a single mixed state simulation was run. This was sufficient to gain a broad understanding of the morphological effects of PCND. Some additional simulations were run with the initial conditions being the results of the mixed state simulations at a chain length of 16 beads. These simulations were run with no PCND. These will be referred to as a post-processing simulations. The reason for running them was that

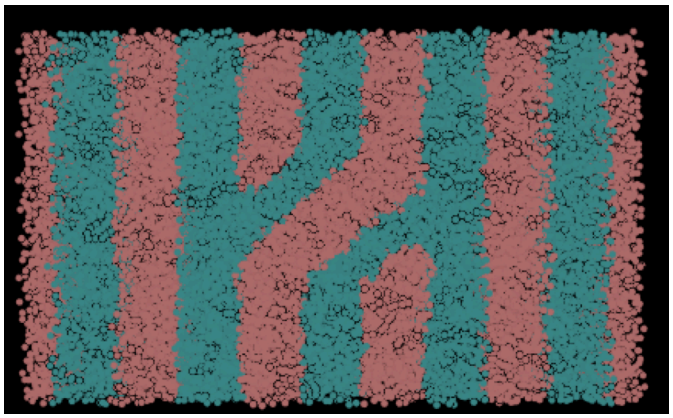

running under non-PCND conditions might correct morphology problems caused by PCND. at 0.5 kcal/mol.

Defective State Studies

The defective state simulations were intended to look at the effect of PCND on the equilibration time of viscous systems. These simulations had initial conditions with an incomplete, as pictured in Figure 6. This is a viscous system, which under normal circumstances would take months of computing to reach equilibrium. The normal equilibrium is a complete lamellae, similar to the mixed state results at equilibrium. All of these simulations were run for the same box size, which was 60.75x36.45x12.15 nm^3 . Two different χ N values of 27, 41.5 and 55, were used for this set of simulations because previous work has shown that computational time required is strongly dependent on the selection of χ N. This parameter was controlled by changing the value of ε_{AB}, the interaction parameter between A and B beads in the simulation. The empirical relationship in Equation 9 was used to estimate the χ as a function of ε_{AB} . ε_{AA} is the interaction parameter between A beads, and this was held constant at 0.5 kcal/mol. N was kept at 64 monomer (which translates to a chain length of 16 beads). Other than the box size and χN, these simulations

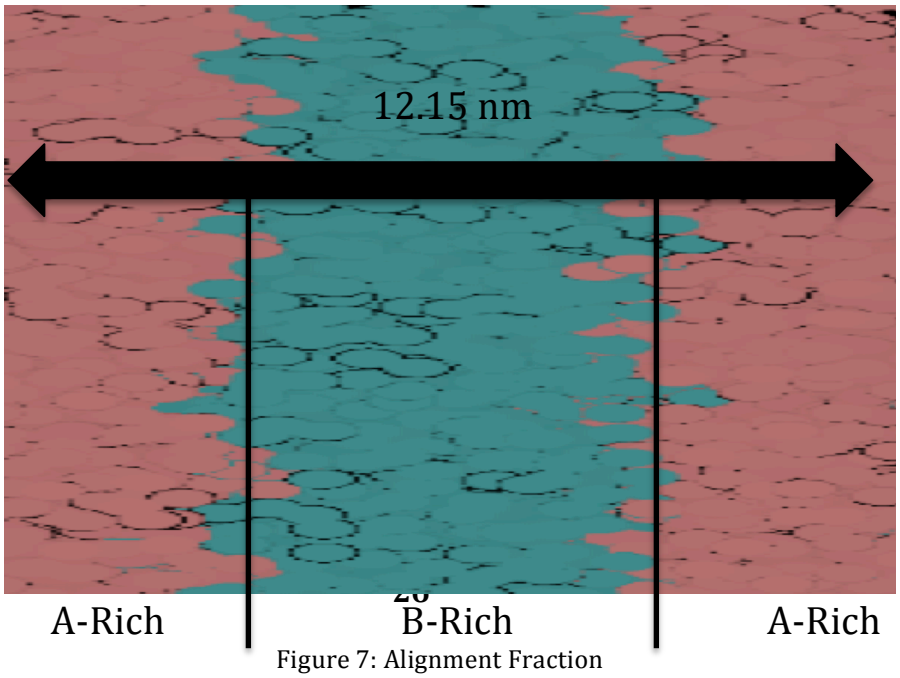

Figure 7: Alignment Fraction

were run under the same conditions as the mixed state, and a similar script as in Appendix A could be used to build either one.

The characterization of these simulations was based on the alignment fraction (f) over time (t). Alignment fraction was measured at discrete time steps. Alignment fraction is the fraction of A and B beads in proper lamellar alignment. This was measured only for the broken lamellae in the center. It was found by examining a single pitch length (12.15 nm was the pitch) in the center of the broken lamellae and then dividing it up into two phase rich regions as pictured in Figure 7. Ideally, if the lamellae was perfectly formed, then the separate phases would contain their respective beads. Three alignments were calculated, one for the center region (B rich phase) and two for each of outer regions (A rich phases). The average of these was taken as the final alignment fraction. Figure 7 provides a visual demonstration of how the quadrants were subdivided. Because of computing limitations, the number of f samples taken for each simulation was relatively small (compared to the U for mixed state studies), with 2500 – 5000 ps of simulated time between each measurement.

The alignment fraction was measured over time, and an equilibrium alignment was calculated. This was done by finding the maximum alignment over time and then averaging alignment from the time of the maximum to the end of the signal. For a limited number of alignment signals, the max alignment was at the end of the signal, in which case the averaging was done over the last five alignment values. The equilibrium time for each simulation was taken as the first time when it passed above the equilibrium alignment fraction. This generally provided qualitatively accurate results, as shown in Figure 8, for a typical alignment profile. Previous work had interpreted the equilibrium time as rate by inverting it. This was done for this study so that the results can be easily compared with

related work. Finally, because of the high variability of the results of these simulations, measurements were averaged over 10-20 different simulation results with the same parameters.

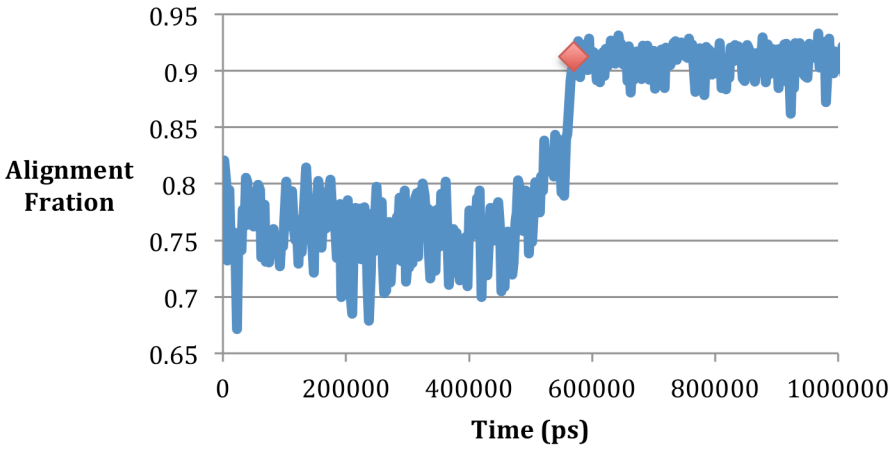

Figure 8: Typical Alignment Fraction Profile Over Time

Chapter 4: Results

Mixed State Studies: Scattering Intensity

Table 3 shows the maximum scattering intensity (I_{norm}) of mixed state non-PCND simulations at equilibrium. Figures 9a, 9b, and 9c present the max scattering intensity (I_{max}) normalized by the I_{norm} for that chain length, of a wide variety of PCND parameters. For a complete listing of all collected results, see Appendix B.

Table 3: Max Scattering Intensity for Non-PCND Simulations

	Chain Length = 16 beads	Chain Length = 24 beads	Chain Length = 32 beads
I_{norm}	201.65	332.97	502.18

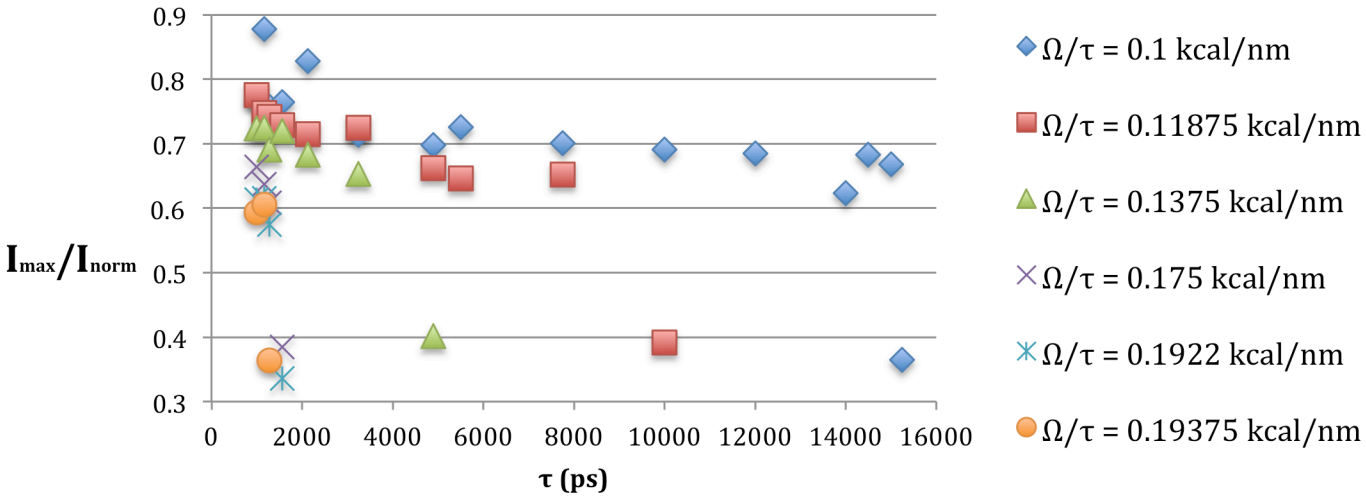

Figure 9a: Normalized Max Intensity for Chain Length = 16 beads

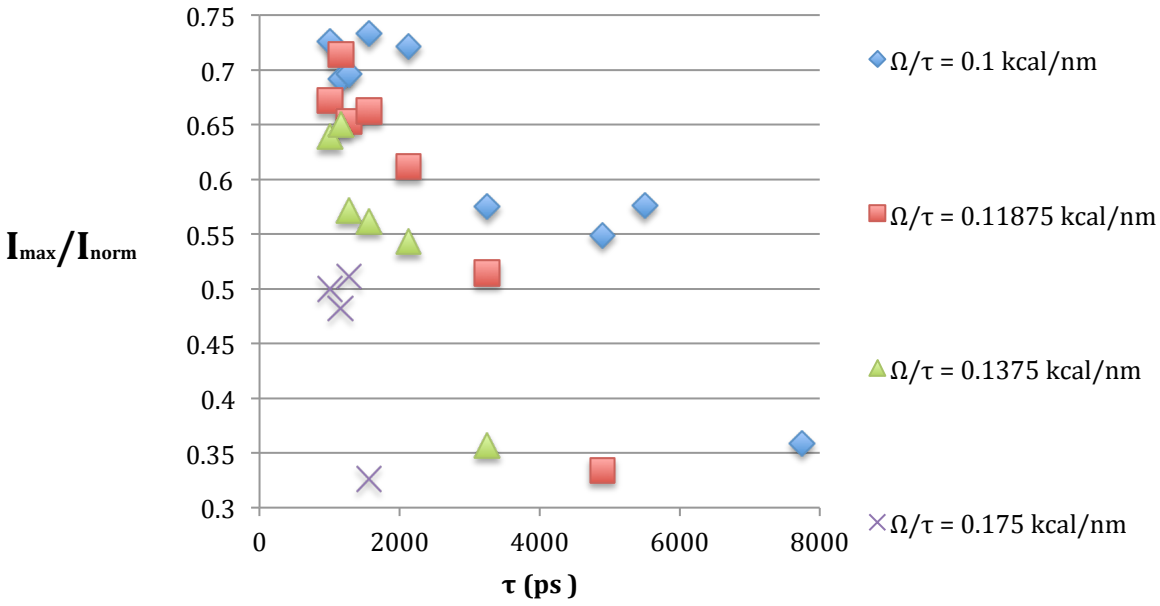

Figure 9b: Normalized Max Intensity For Chain Length = 24 beads

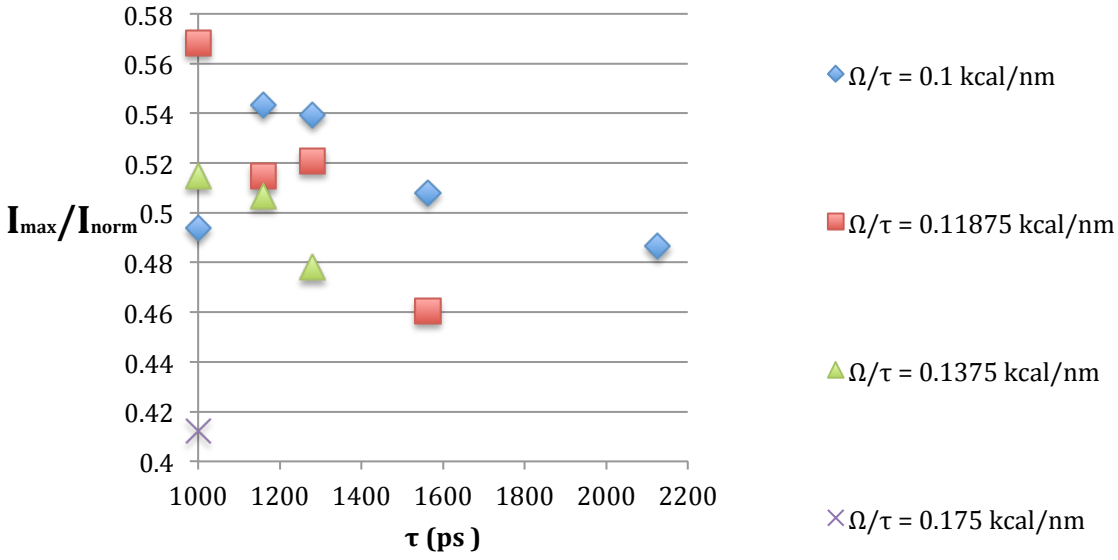

Figure 9c: Normalized Max Intensity For Chain Length = 32 beads

Figure 10 shows the region of Ω/τ and τ values that maintained lamellae formation at equilibrium. The upper boundaries of the threshold were defined as the parameters that caused normalized intensity to drop below 0.5 (which means it was less than half the intensity of the non-PCND).

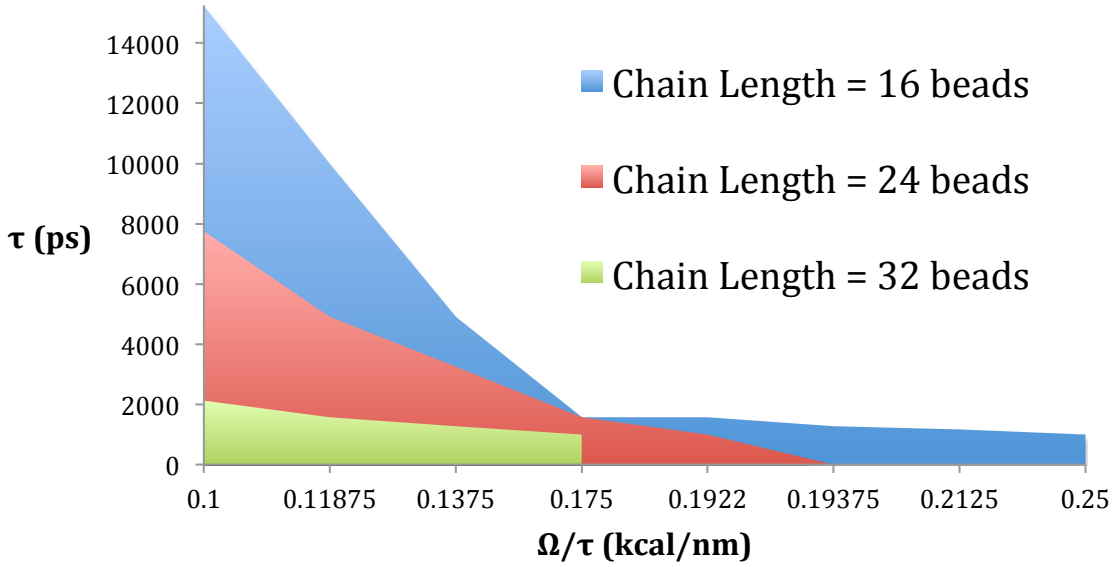

Figure 10: Upper Threshold on PCND Parameters for Mixed State Simulations

The results of post-processing on normalized intensity of mixed state simulations is shown in Figure 11. This includes the results for most of the post processing simulations that were run. Comprehensive results can be found in Appendix B.

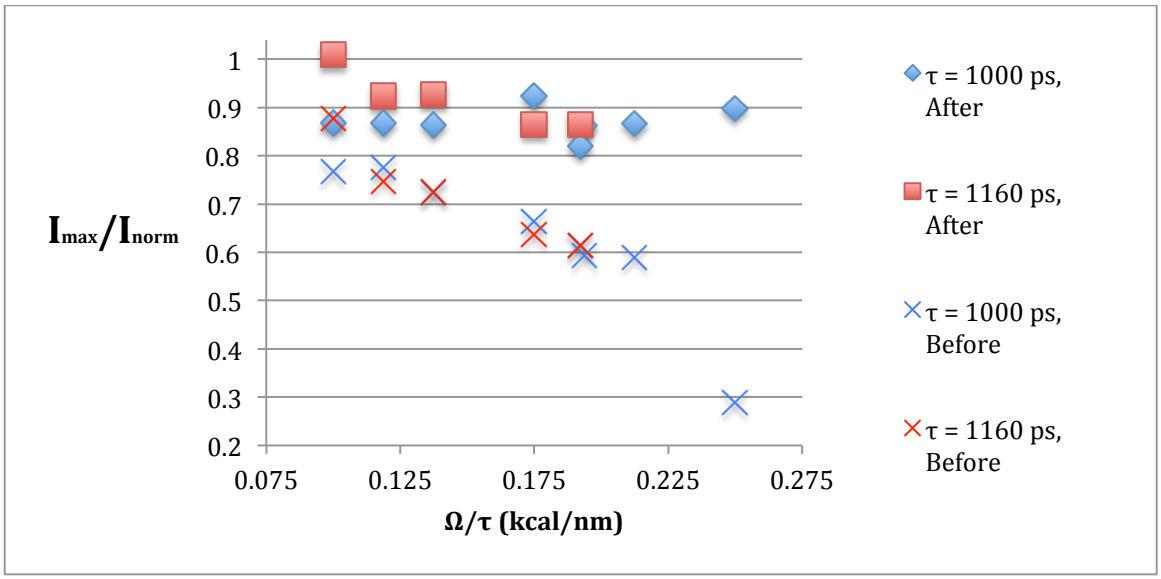

Figure 11: Normalized Intensity Before and After Post-processing

Mixed State Studies: Pitch Measurements

The equilibrium pitch of mixed state simulations for a wide range of parameters are shown in Figures 12a-d. The black line shows the equilibrium pitch of a non-PCND simulation for comparison.

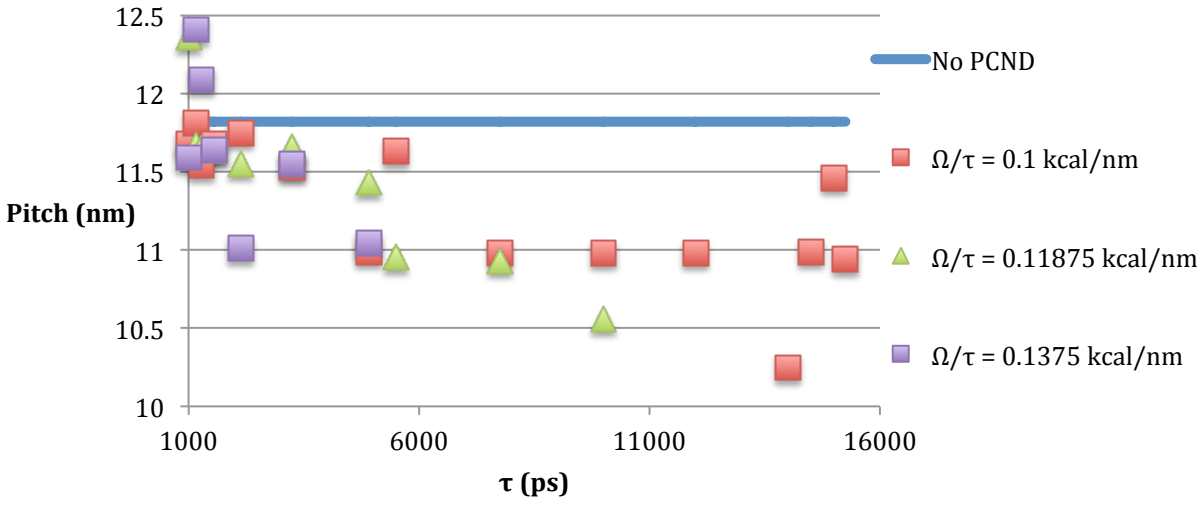

Figure 12a: Equilibrium Pitch For Chain Length = 16 beads

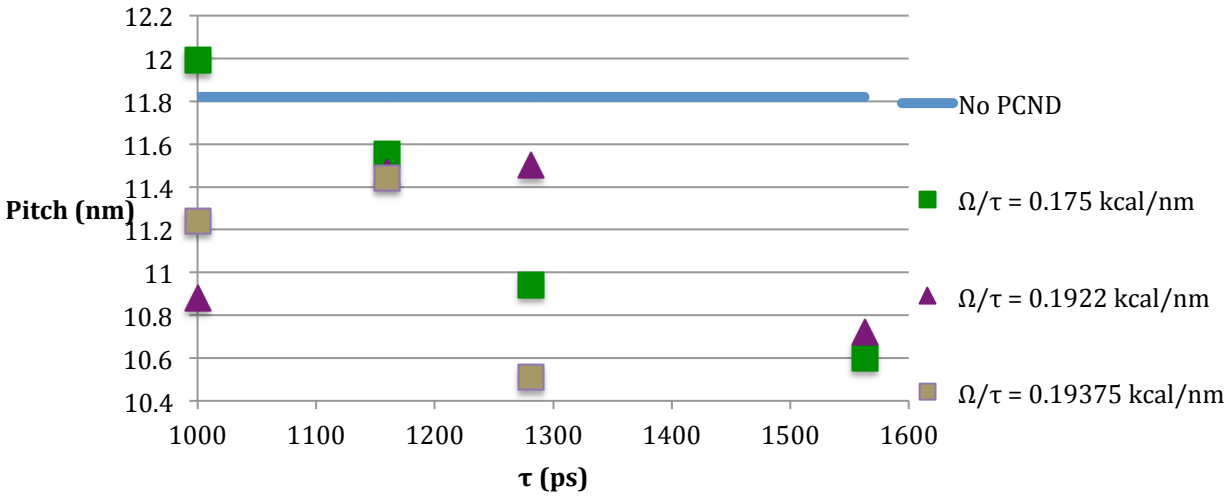

Figure 12b: Equilibrium Pitch For Chain Length = 16 beads, cont.

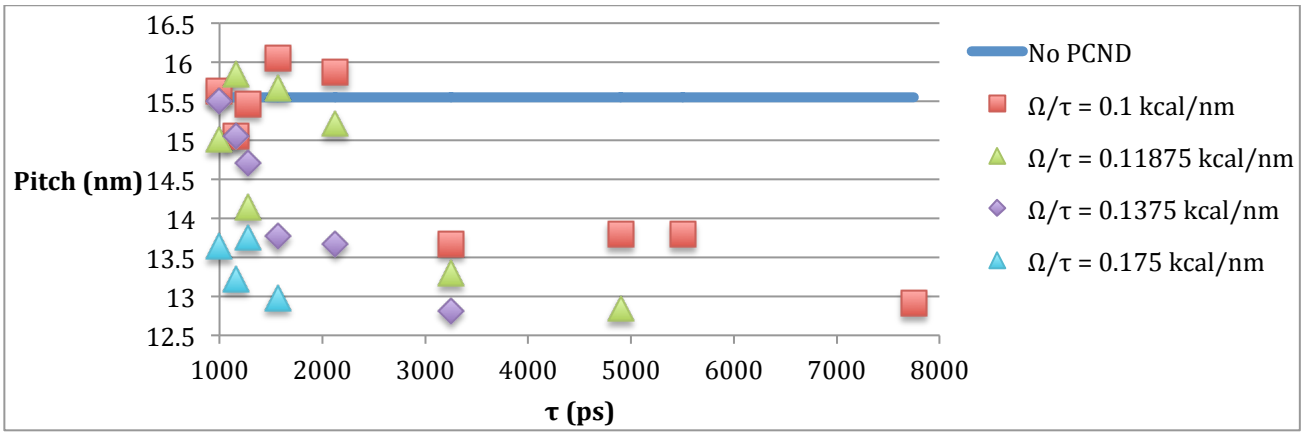

Figure 12c: Equilibrium Pitch For Chain Length = 24 beads

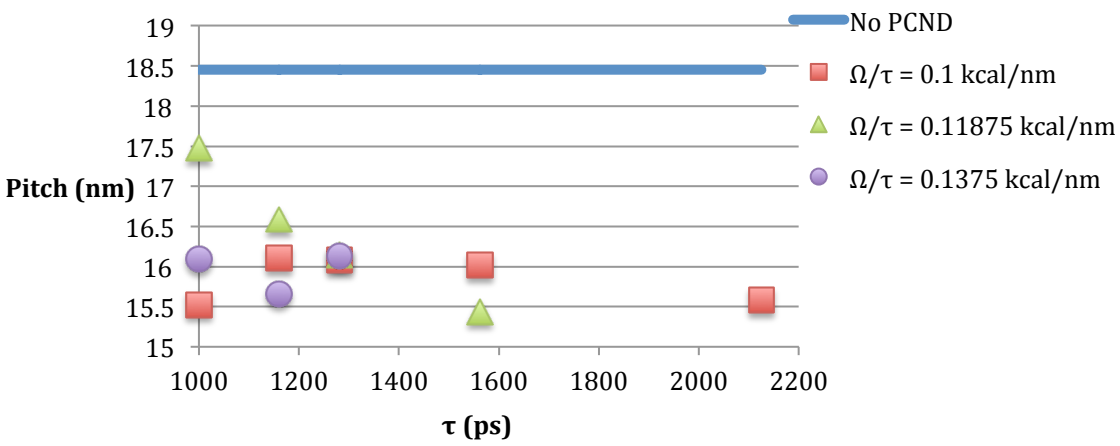

Figure 12d: Equilibrium Pitch For Chain Length = 32 beads

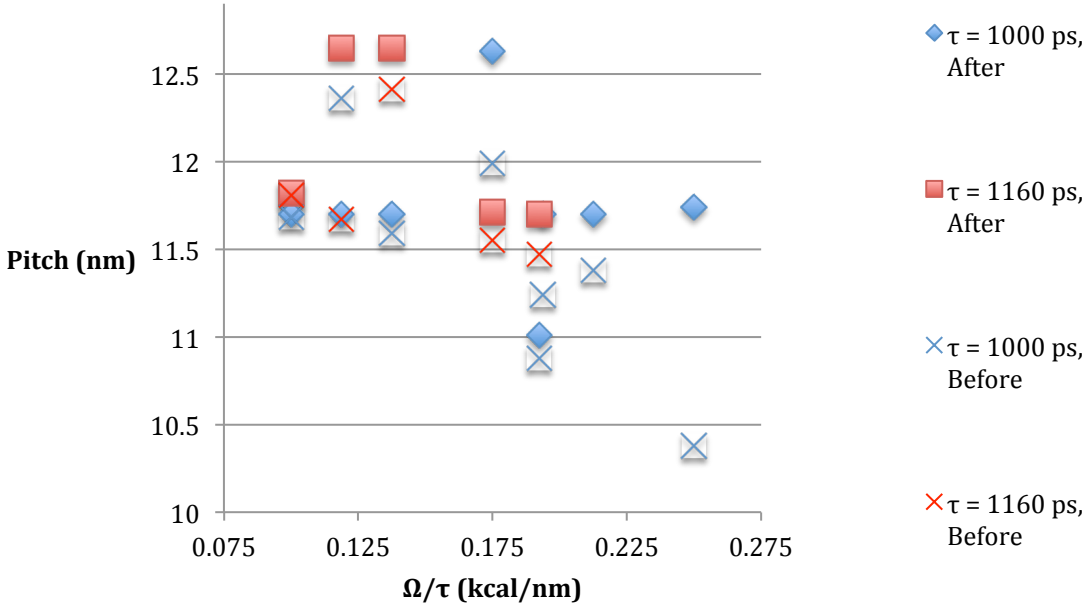

Figure 13: Pitch Before and After Post-Processing

Mixed State Studies: Equilibrium Time Step Measurements

Figures 14a-14d show the equilibrium time step measured for a wide variety of parameter values.

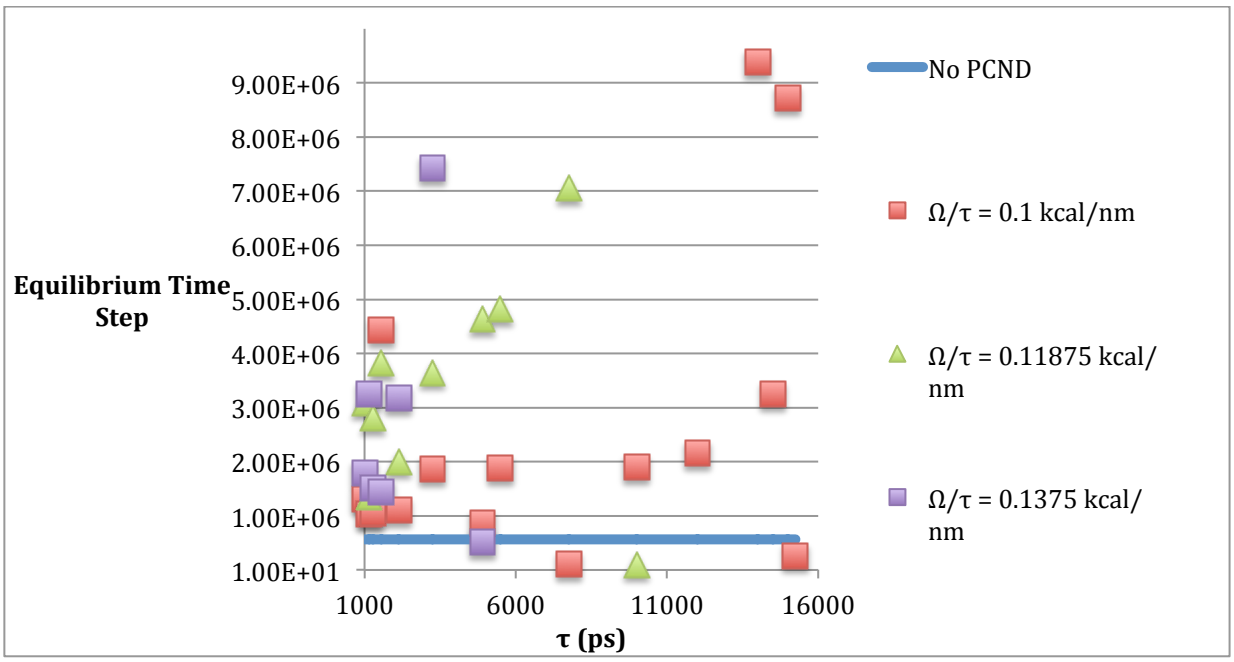

Figure 14a: Equilibrium Time Step Chain Length = 16 beads

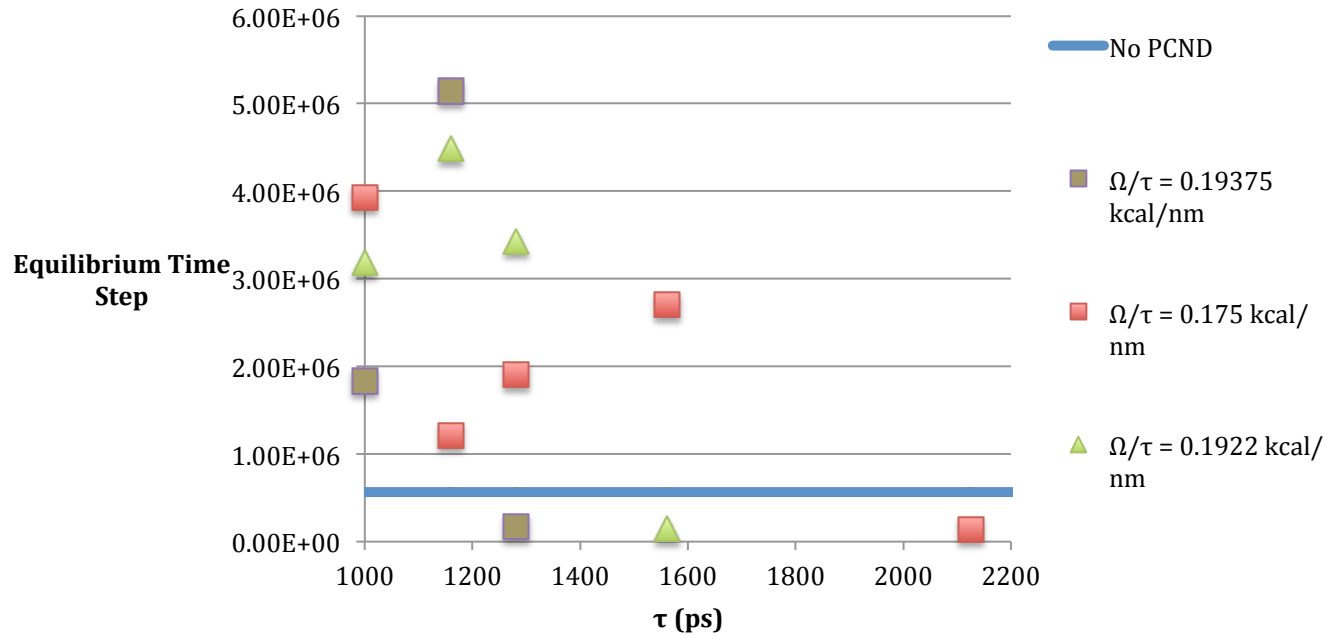

Figure 14b: Equilibrium Time Step Chain Length = 16 beads, cont.

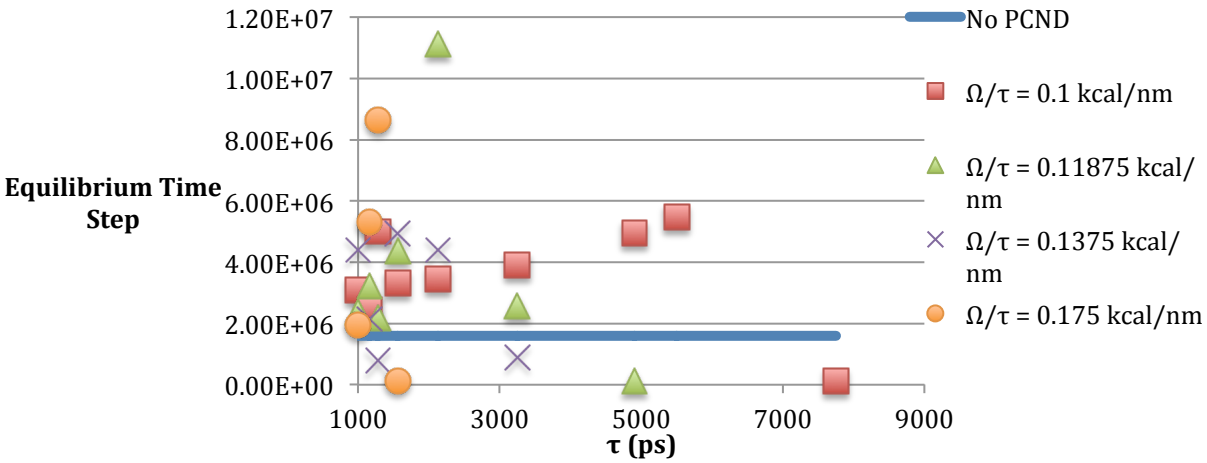

Figure 14c: Equilibrium Time Step Chain Length = 24 beads

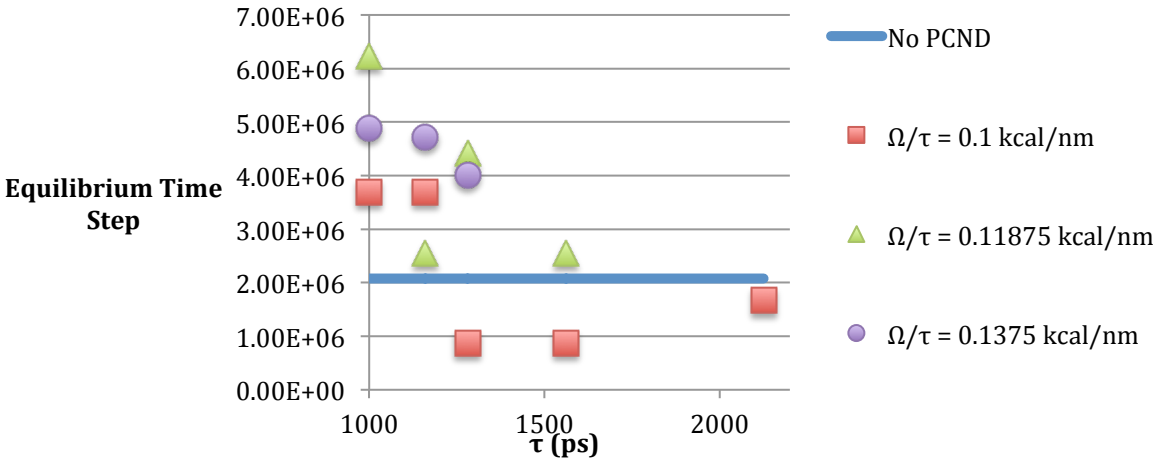

Figure 14d: Equilibrium Time Step Chain Length = 32 beads

Results: Defective State Studies

Figure 15a and 15b show the equilibrium alignment and annealing rate respectively, for defective state simulations with a wide variety PCND parameters. Because multiple runs of each simulation were done, the results shown are averages with error bars of 95% confidence intervals.

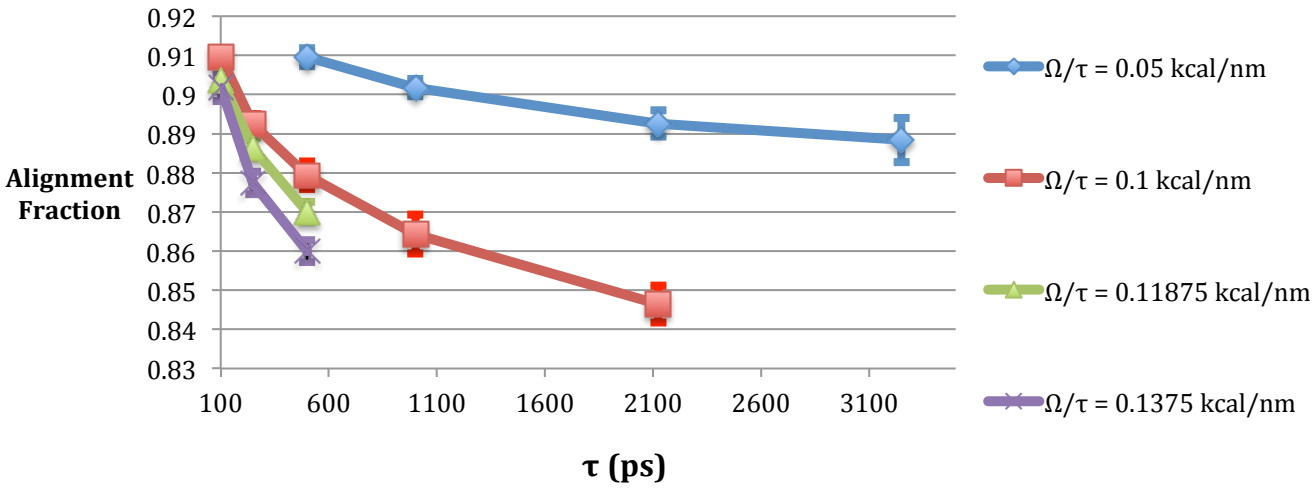

Figure 15a: Average Equilibrium Alignment Fractions to 95% Confidence at $\chi N = 55$

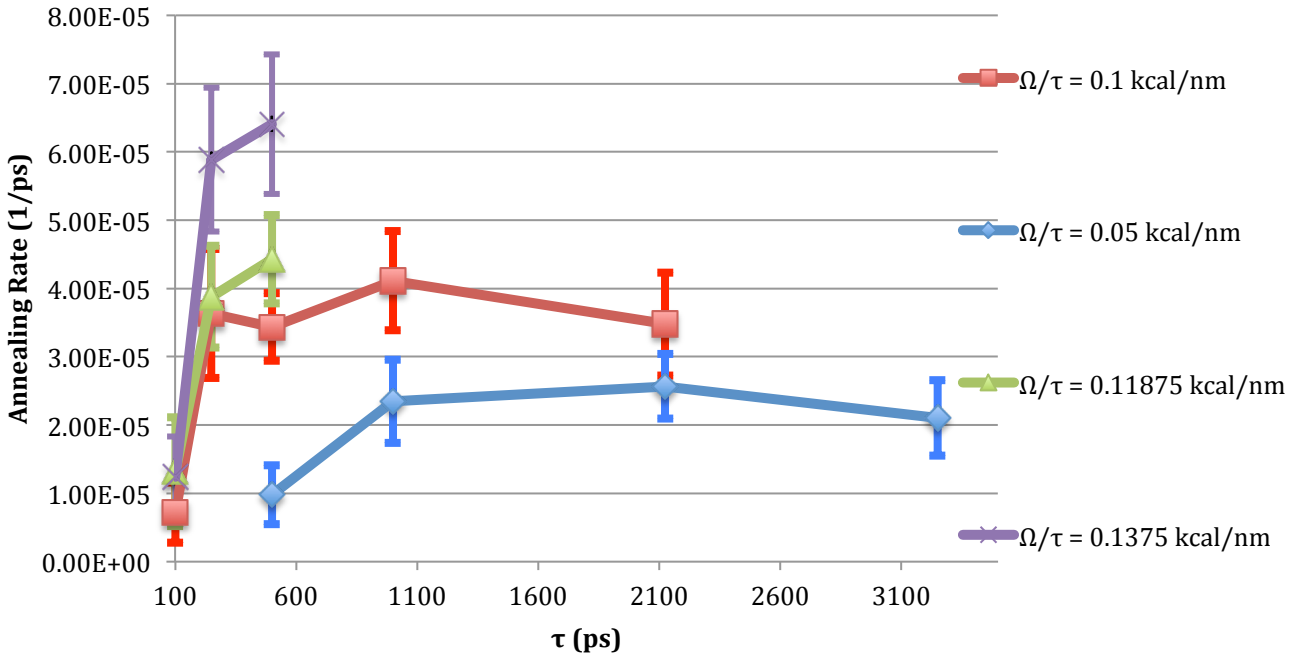

Figure 15b: Average Annealing Rates to 95% Confidence at $\chi N = 55$

Figure 16 provides a comparison of the equilibrium alignment fractions as a function of χN, for several values of Ω/τ and τ. Figure 17 compares PCND annealing rates at two χN (41.5 and 55) with results for non-PCND results at much lower χN. The best fit straight line shows an approximate extrapolation from the non-PCND results. The reason for only using 2 χN is because the calculation for annealing rate for $\chi N = 27$ was negative, and so it would not be relevant for comparison.

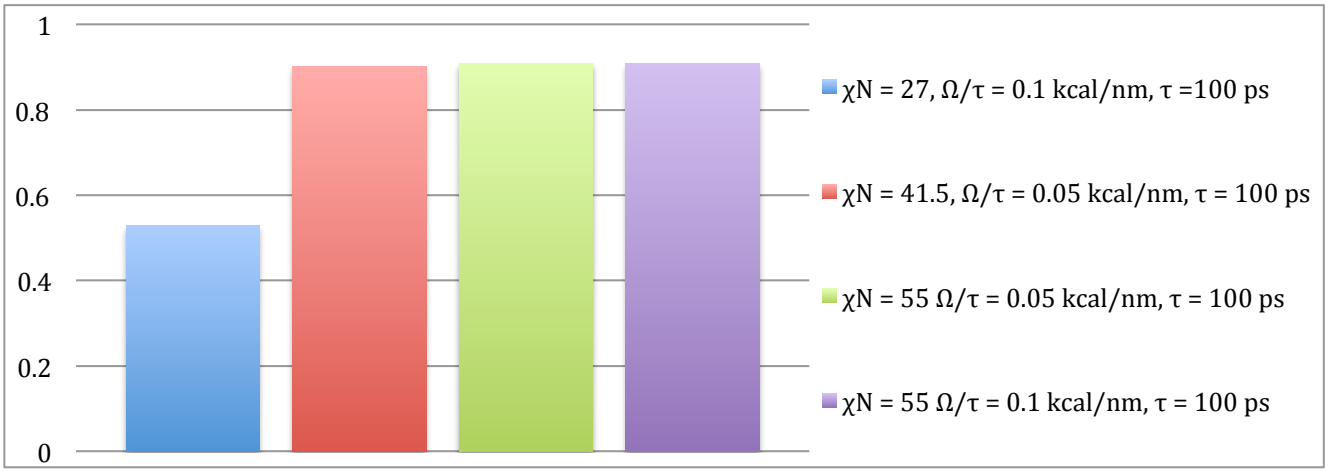

Figure 16: Alignment Fractions as a Function of χN

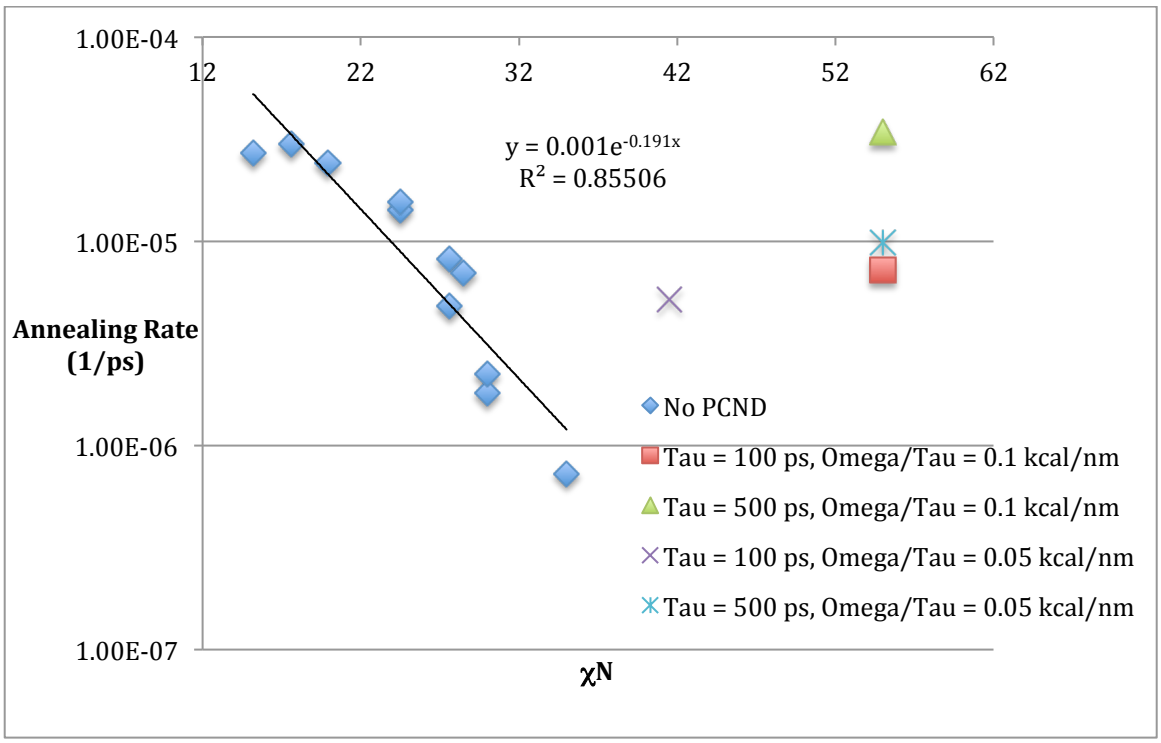

Figure 17: Annealing Rate as a Function of χN For PCND and Conventional MD

Chapter 5: Discussion

Mixed State Studies

The trend for intensity is that as either Ω/τ or τ is increased, the intensity decreases. Since increasing either parameter should result in higher magnitude random forces, the decline seems to reflect increasing disorder of lamellae with increasing noise. This is illustrated with Figure 18, which shows visually what the result of increasing either parameter. As either is increased, the lamellae become more dispersed and bent. At the

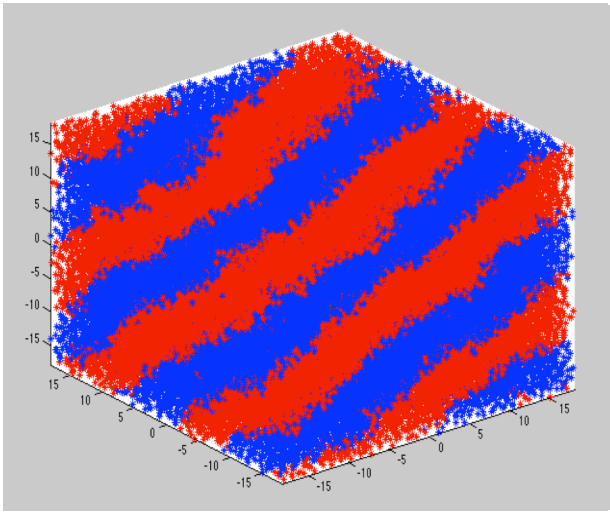

Ω/τ = 0.11875 kcal/nm, τ = 1000 ps

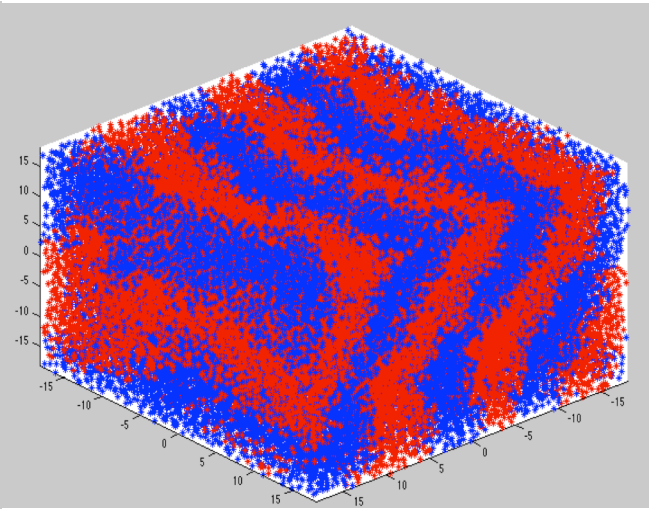

Ω/τ = 0.11875 kcal/nm, τ = 4900 ps

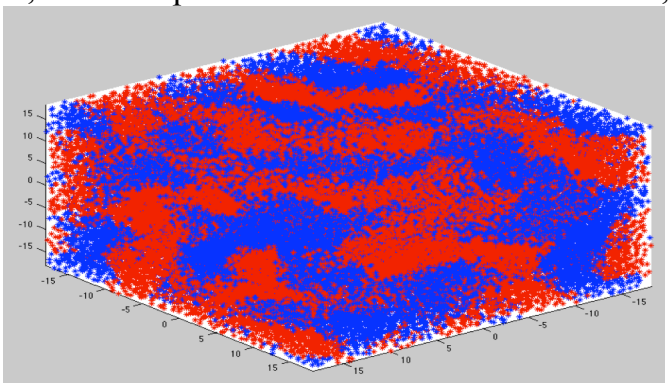

Ω/τ = 0.1375 kcal/nm, τ = 4900 ps

Figure 18: Qualitative Result of Increasing Either PCND Parameter At Chain Length = 16

threshold of the PCND parameters, the lamellae are completely absent. This suggests that increasing noise causes greater disorder and coarseness in lamellae.

The intensity results in Figure 9a provide the steepest cutoff for PCND parameters. As τ increases at constant Ω/τ, the normalized intensity declines steadily, but at extreme values, it drops suddenly to below 0.5, and that is associated with the failure to form lamellae. This represents the point at which random PCND induced motion dominates normal polymer behavior. Figure 10 shows that the threshold occurs while increasing either of Ω/τ or τ, so both parameters ought to be kept safely below that limit.

Figure 10 also shows that the threshold parameter space gets smaller for increasing chain length. This result is unsurprising since large molecular weight polymers have a strong tendency to get trapped in disordered states, meaning that smaller magnitudes of noise have much stronger effects.

The minimum peak scattering intensity to form lamellae was originally based on results from chain length = 16 results, which indicated a clear transition for increasing noise. The transition becomes less obvious for larger chain lengths, and some results did form lamellae even when the intensity was slightly below 0.5, such as the result for chain length = 32, Ω/τ = 0.1 kcal/nm, and τ = 1000 ps. This suggests that the minimum intensity to form lamellae may be lower for larger chain lengths.

The flatness of the normalized intensity curve for chain length = 32 suggest that at larger chain lengths, a more detailed sampling was needed, and as result, the threshold for chain length = 32 is a more coarse approximation then the one for 16 beads. Becuase values at the threhold failed to form lamellae, we can safely say that a more accurate approximation would only go to lower PCND parameters. Even though the approximation is slightly

inaccurate, the overarching trend of reduced parameter space for increased chain length would not be any different for better sampling.

Furthermore, the results suggest that larger PCND parameters induce greater disorder in lamellar shape, even for values below the threshold. Lamellae achieve significantly better alignment at normalized intensities well above 0.5. Therefore, ideal PCND parameters for BCP systems are well below the threshold limits found for these mixed state simulations.

The post processing results show an increase in normalized intensity relative to the PCND results. The qualitative results are shown in Figure 19. After non-PCND running, the roughness of the lamellae is reduced. This suggests that running with non-PCND can correct the disorder that was induced by PCND. The limitation is that the correction is incomplete near the threshold values. If the PCND produces lamellae at all, then the lamellae can be smoothed by running the results using conventional MD. When simulations fail to form lamellae, the induced disorder can be partially corrected but not completely. The conclusion is that post processing can correct minor edge roughness, which tends to be produced by

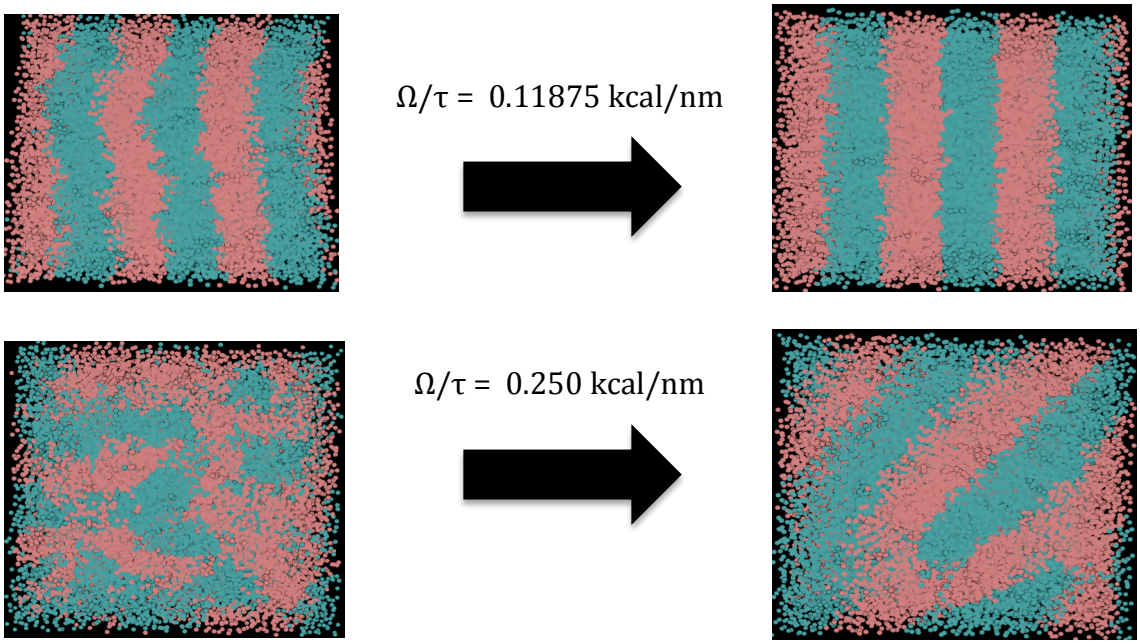

Figure 19: Corrective Effect of Post-Processing at τ = 1000 ps

moderate PCND parameters.

The pitch results show a general decrease for large increases in PCND parameters. This is explained by two factors. First, as was discussed above, the lamellae generally became rougher and bent as noise increased. Since the pitch calculation was based on the assumption that the lamellae were perfectly uniform, the reduced pitch is partially a reflection of the error of that assumption for highly rough results. The second factor is the changes in tilt of the lamellae. Returning to Figure 4b, as noise increased, the tilt of the lamellae relative to the simulation box changed. Increasing tilt results in lower pitch.

One of the limitations on the pitch results is that they were strongly influenced by box size. Certain PCND results actually achieve higher pitch than non-PCND simulations. As we see in Figure 4b, moderate values PCND parameters produced lamellae that were closer to parallel with the sides of the simulation box, which explains the higher pitch. It is likely that the box sizes used constrained the possible pitches that the polymers could achieve naturally (in the absence of random forces). Ideally, the box dimensions should not have been a relevant parameter, but that would have required significantly larger boxes. Because of limitations on available computing power, it was not possible to explore larger box sizes without drastically lowering the bead density. Future studies may seek to look at larger box sizes so that pitches will be less constrained.

The post-processing results at a chain length of 16 show reduced variation in the pitches. Most of the pitches were around 11.7 nm, which is extremely close to the non-PCND value of 11.8 nm. Most of the other values ended near 12.65 nm or 11.01 nm. We know from the intensity results that the post-processing corrected some roughness, which did affect the pitch results for PCND. With corrected roughness, the small variations in pitch vanish, and

the only factor that affects pitch is the tilt. The commonly observed pitches for post-processing represent the pitch, when it is only affected by the tilt of the lamellae. The relatively small number of common pitch lengths, suggest that there may only be several possible tilted shapes for straight lamellae. This may be dependent on box dimensions.

The equilibrium time measurements indicate that with very few exceptions, the PCND results equilibrated at a slower rate compared to the non-PCND. This was due to the fact that the mixed state simulations started from a high potential energy state. As a result, the driving force for these simulations to form lamellae was already incredibly high. Because the random forces fluctuated heavily over a relatively large time scale, the simulations potential energy was kept relatively high until the random forces dissipated. If the correlated forces dissipated at a rate faster than the potential energy of the simulation, then it is possible that this elevated potential energy might not have been sustained. Since the dissipation of random forces can be controlled by τ, this problem might be resolved by reducing that parameter. Furthermore, it should be noted that the potential energy of the systems decreased so quickly for all mixed state simulations that for most of their run time, they are near equilibrium potential. PCND induced longer pseudo-equilibrium states, which delayed the true equilibrium but not by a significant of potential energy.

Defective State Studies

Figure 17 shows that although higher χN usually results in lower annealing rates, the PCND simulations show similar or increased annealing rates. The consequences of this for real time computing are substantial, since large χN were previously inaccessible due to slow computing speed. Typical simulations with PCND took 12-48 hrs to come to equilibrium,

which is an improvement by several orders of magnitude. Figure 15b shows that there is some variance in the annealing rates, but this additional randomness was small relative to the improvement in computing speed. We also see that there are optimal regions for τ at constant Ω/τ, as was earlier seen by Jenkins for a single particle.

The alignment fraction results in Figure 15a show that for increasing noise, the alignmnent of the lamellae decreases. This indicates increased lamellaer roughness and reduced staightness. Similar to the results for the mixed state simulations, as the noise increases, the coarseness of the lamelllae also increases. Considering that the initial alignment was around 0.82 for all simulations, the final alignment for large PCND parameters is a relatively small improvement. Because of the reduced alignment at high PCND parameters, it seems advisible to use only the smaller parameters for Ω/τ and τ. This would seem to be acceptable, since even smaller parameters achieved a very fast annealing rate.

Figure 16 shows that for relatively similar noise levels, the lamellae achieve lower alignment for lower χN. This is an unsurprising result, since χN is the resistance to phase separation, which means that lower χN will have a greater tendency toward instability and disorder. We can say then that lower noise levels would be necessary to achieve higher alignment for lower χN.

Annealing rate data generally shows an exponential drop with increasing χN, but this trend to seems to be broken with the application of PCND. Although there is only one data point for $\chi N = 41.5$ this shows a reduced annealing rate compared to the $\chi N = 55$ results. One possible explanation for this outcome is that applying PCND flattens the χN dependence. This is supported by the fact that increasing noise (e.g. by increasing Ω/τ from

0.05 to 0.1 kcal/nm) seems to have a stronger effect on annealing rate than increasing χN from 41.5 to 55. With the collection of more data points at a wider range of χN, this may become more evident. It is strongly recommended that future research investigate more fully the dependence of PCND annealing rates on χN.

Chapter 6: Conclusions

The goal of this study was to investigate the effectiveness PCND as an alternative to conventional MD for simulations of diblock copolymers. Two effects were investigated: effects on morphology and effects on the speed up. A large number of simulation results were compiled and analyzed, and the two effects were characterized. The investigation of the first effect found that as intensity of random forces was increased, the roughness and disorder of the lamellae increased. The lamellae also experienced tilt when compared to non-PCND results. A threshold was developed for determining what PCND parameters produced non-lamellar results. In this way, a useful parameter space for PCND was developed. The primary effect of chain length on these results appears to be that as chain length increases, the useful parameter space becomes compressed. In the future, it is suggested to investigate a more detailed parameter space, with increased sampling of Ω/τ and τ at larger chain lengths.

Edge roughness of the lamellae can be significantly corrected using non-PCND methods after PCND, but this will not completely correct a non-lamellar or tilted condition.

The investigation of speed up effects found that for kinetically uninhibited systems, there was no reduction in equilibration time, which means PCND is not helpful when applied to these systems. However, when applied to a high activation energy simulation, the effect was enormous. Annealing rates increased by several orders of magnitude, even for small noise intensities. Furthermore, there appears to be optimal τ for constant Ω/τ, which confirms the earlier result by Jenkins. Furthermore, it seems that the PCND parameters have a stronger effect on annealing rate than χN, which is significant because the annealing rate in conventional MD is heavily dependent on χN. That said, larger PCND noise levels resulted in significantly decreased alignment at equilibrium, which suggests that these are not useful.

The computational time reduction for kinetically inhibited systems is the most important result from this study. It is strongly recommended to continue the exploration Ω/τ and τ for a wide variety of χN. The χN dependence observed in this study is extremely interested and warrants further study.

Appendix A: Complete Sample HOOMD Script

```
#hoomd_script::init::read_xml hoomd_script::dump::dcd hoomd_script::pair::lj #hoomd_script::bond::harmonic
hoomd_script::integrate::mode_standard #hoomd_script::integrate::nvt
# Due to deficiencies in doxygen, the commands used in this example are listed explicitly here
# run this script with "python -x filename" to skip the first line, or remove this header
# ---- init_xml.py ----
from hoomd_script import *
import math
from hoomd_plugins import pair_ext_template
# Intrinsic Units for Conversion
intr_L = 1   #1 nm
intr_E = 1  #1 kcal/mol
intr_tau = 1 # 1 ps
intr_T = 0.001987  #1 / K
intr_P = 0.06857 #1/atm
###---### Input Parameters ###---###
inputfilename = "" #input file name with initial state
import os
prefix=os.getenv("HOME")
outputnamestart = prefix+"/Public/“ #Name of output file
T = 500  #K
P = 1  #atm5
timemax = 600000  #ps
timestep = 0.05  #ps
savetime = 5000  #ps
logtime = 25  #ps
n_chains = 2790  #number of chains
```

```
omega_tau2 = 0.1  #omega over tau kcal/nm

tau2 = 1160 #ps

#Constants for bond/angular/LJ interactions

sigAA = 1.26  #nm

epsAA = 0.5  #kcal/mol

sigBB = 1.26  #nm

epsBB = 0.5  #kcal/mol

sigAB = 1.26  #nm

epsAB = 0.3  #kcal/mol

Laa = 0.82  #nm

kstraa = 100  #kcal/mol/nm^2

Lbb = 0.82  #nm

kstrbb = 100  #kcal/mol/nm^2

Aaaa = 120  #degrees

kangaaa = 5  #kcal/mol/radians^2

Abbb = 120  #degrees

kangbbb = 5  #kcal/mol/radians^2

potentialtype = 84  #84 or 63

LJcutoff = 4  #nm

###---### End Input Parameters ###---###

#convert parameters to hoomd intrinsic parameters

T = intr_T * T

P = intr_P * P

savetime = savetime/timestep #convert to number of timesteps between saves

logtime = logtime/timestep

timemax = timemax/timestep + 1 #convert to number of timesteps total +1 to allow final timestep to write to
file.

Aaaa = Aaaa*math.pi/180  #convert to radians
```

```
Abbb = Abbb*math.pi/180  #convert to radians
#Print any desired parameters
print ""
print(savetime)
print ""
########################################################################
o_t=omega_tau2 #omega over tau
t=tau2 #tau
tau=t
omega_tau=o_t
outputname=outputnamestart+'_'+str(omega_tau)+'_'+str(tau)+'_1' #Output naming
print outputname
# read in the file
init.read_xml(filename=inputfilename)
### Force Field Setup ###
#Turns on bonds and angles
harmonic = bond.harmonic()
angleharmonic=angle.harmonic()
#Sets bonds and angles properties
# Every thing param. must be in system and no extras.
#Stretching parameters
harmonic.set_coeff('polymer', k=kstraa, r0=Laa)
harmonic.set_coeff('polymer2', k=kstrbb, r0=Lbb)
#Angles parameters
angleharmonic.set_coeff('A-A-A', k=kangaaa, t0=Aaaa)
angleharmonic.set_coeff('B-B-B', k=kangbbb, t0=Abbb)
n = n_chains+1
```

```
for x in range(1,n,1):
        angleharmonic.set_coeff('polymer' + str(x), k=0, t0=1)
anglepcnd=angle.cgcmm()
anglepcnd.set_coeff('A-A-A', omega_tau=0, tau=1,timestep=timestep,total_chains=n_chains,chain_number=1)
anglepcnd.set_coeff('B-B-B', omega_tau=0, tau=1,timestep=timestep,total_chains=n_chains,chain_number=1)
for y in range(1,n,1):
        anglepcnd.set_coeff('polymer' +str(y),omega_tau=omega_tau,
tau=tau,timestep=timestep,total_chains=n_chains,chain_number=y)
print tau
print omega_tau
sorter.disable()
#update.zero_momentum()
zeroer= update.zero_momentum(period=10)
# Lennard Jones parameters     # Always set alpha to 2 to maintain same potential as in moe. (minimum at
sigma)
if potentialtype == 63:
        lj = pair.lj(r_cut=LJcutoff)  #Run for 6,3 potential uncomment
else:
        lj = pair_ext_template.pair.lj2(r_cut=LJcutoff)  #Run for 8,4 potential uncomment
lj.pair_coeff.set('A', 'A', epsilon=epsAA, sigma=sigAA, alpha=2)
lj.pair_coeff.set('B', 'B', epsilon=epsBB, sigma=sigBB,alpha=2)
lj.pair_coeff.set('A', 'B', epsilon=epsAB, sigma=sigAB, alpha=2)
#exclusions to LJ calc.
nlist.reset_exclusions(exclusions=['1-2', '1-3'])  # check for error
#nlist.reset_exclusions(exclusions=['1-2', '1-3', '1-4'])
#nlist.set_params(dist_check=False,r_buff=0.1)
### End Force Field Setup ###
all = group.all()  #groups everything as all
```

```
#### New Minimizer
Laa = 0.82  #nm
Lbb = 0.82  #nm
kstraa = 1000000  #kcal/mol/nm^2
kstrbb = 1000000  #kcal/mol/nm^2
fire=integrate.mode_minimize_fire(group=all, dt=0.000005, ftol=1e-2, Etol=1e-7, finc=1.99, fdec=0.8,
alpha_start=0.01, falpha=0.9)
for step in range(1,1261,50):
        sig=float(step)/1000
        lj.pair_coeff.set('A', 'A', epsilon=epsAA, sigma=sig, alpha=2)
        lj.pair_coeff.set('B', 'B', epsilon=epsBB, sigma=sig, alpha=2)
        lj.pair_coeff.set('A', 'B', epsilon=epsAB, sigma=sig, alpha=2)
        fire=integrate.mode_minimize_fire(group=all, dt=0.000005, ftol=1e-2, Etol=1e-7, finc=1.99, fdec=0.8,
alpha_start=0.01, falpha=0.9)
        run(50)
        dump.xml(filename=outputname+"_HOOMDMinimized.xml", vis=True)
#### Old Minimizer
sig=1.26
lj.pair_coeff.set('A', 'A', epsilon=epsAA, sigma=sig, alpha=2)
lj.pair_coeff.set('B', 'B', epsilon=epsBB, sigma=sig, alpha=2)
lj.pair_coeff.set('A', 'B', epsilon=epsAB, sigma=sig, alpha=2)
Laa = 0.82  #nm
Lbb = 0.82  #nm
kstraa = 100  #kcal/mol/nm^2
kstrbb = 100  #kcal/mol/nm^2
#dump.xml("rnBx1.xml", vis=True)
```

```
fire=integrate.mode_minimize_fire(group=all, dt=0.00005, ftol=1e-2, Etol=1e-7, finc=1.99, fdec=0.8,
alpha_start=0.01, falpha=0.9)
run(20000)
#Setup how often the simulation prints the data
##Dumps the initial configuration.
dump.xml(filename=outputname+".xml", vis=True)
#dump.mol2(filename=outputname)
#Dumps data every period number of timesteps
dump.dcd(filename=outputname+".dcd", period=savetime)
##dcd is for visualization in VCD
dump.xml(filename=outputname+".xml", vis=True, period=savetime*6)
##xml is the intrinsic file format
#dump.mol2(filename=outputname, period=savetime)  #mol2 is a format that moe can read
# Run dynamics for a desired number of time steps
#c=compute.thermo(group=all)
analyze.log(quantities=['temperature','pressure','volume','potential_energy','kinetic_energy','pair_lj_energy','bon
d_harmonic_energy','angle_harmonic_energy','angle_cgcmm_energy'], period=logtime,
filename=outputname+".log")
integrate.mode_standard(dt=timestep)
integrate.nvt(group=all, T=T, tau=0.2)
##tau is temperature controller parameter
#integrate.npt(group=all, T=T, tau=0.2, tauP=0.5, P=P)
##tauP is pressure controller parameter
run(timemax)
#run(2000,profile=True)
##Command to run desired number of times steps
##delete and reset
```

```
#del lj

#del harmonic

#del anglepcnd

#del angleharmonic

#del all

#del zeroer

#init.reset()
```

Appendix B: Complete Tables of Mixed State Results

Table B1: Chain Length = 16 beads, Equilibration Times in timesteps

τ (ps)	Ω/τ (kcal/nm) No PCND	565300	0.1	0.11875	0.1375	0.175	0.1922	0.19375	0.2125	0.25	0.325	0.4
1000			1317800	3087800	1784300	3927300	3181300	1831800	3438800	92300	185800	79300
1160			1037800	1349800	3245300	1212800	4487800	5141300	129300			
1281.25			1061300	2805800	1516300	1907300	3428300	166300				
1562.5			4425800	3823300	1438800	2698800	145300	132300				
2125			1099800	2005800	3172800	140800						
3250			1856300	3650800	7435300	464800						170300
4900			867800	4635800	509800							
5500			1881300	4819300	110300	153800						
7750			107300	7050300		96800						
10000			1901300	102300								
12000			2151800									
14000			9386800									
14500			3241800									
15000			8718800									
15250			267300									

Table B2: Chain Length = 16 beads, Pitches in nm

τ (ps)	Ω/τ (kcal/nm)	No PCND 11.82	0.1	0.11875	0.1375	0.175	0.1922	0.19375	0.2125	0.25	0.325	0.4
1000			11.68	12.36	11.59	11.99	10.88	11.24	11.38	10.38	9.87	9.57
1160			11.81	11.67	12.41	11.55	11.47	11.44	10.6			
1281.25			11.54	11.65	12.09	10.94	11.5	10.51				
1562.5			11.68	11.64	11.64	10.6	10.72	10.42				
2125			11.75	11.55	11.01	10.05						
3250			11.53	11.66	11.55	10.56						9.17
4900			10.99	11.43	11.04							
5500			11.63	10.95	10.63	10.5						
7750			10.98	10.93		10.52						
10000			10.98	10.56								
12000			10.98									
14000			10.25									
14500			10.99									
15000			11.46									
15250			10.94									

Table B3: Chain Length = 16 beads, Max X-ray Scattering Intensity

τ (ps) \ Ω/τ (kcal/nm)	No PCND	0.1	0.11875	0.1375	0.175	0.1922	0.19375	0.2125	0.25	0.325	0.4
	201.65										
1000		154.66	156.25	145.88	133.85	123.68	119.67	118.95	58.18	40.71	34
1160		176.99	150.7	146.11	128.43	124	122.14	70.65			
1281.25		152.76	149.51	139.39	122.6	115.78	73.33				
1562.5		154.07	146.92	145.16	77.46	67.72	67.77				
2125		166.87	144.08	137.62	71.2						
3250		143.9	146.02	131.74	67.44						33.35
4900		140.65	133.38	80.92							
5500		146.28	130.34	66.42	56.73						
7750		141.23	131.55		62.64						
10000		139.38	78.93								
12000		138.07									
14000		125.62									
14500		137.59									
15000		134.65									
15250		73.48									

Table B4: Post-processing Pitchs in nm

τ (ps) \ Ω/τ (kcal/nm)	Control (no PCND)	0.1	0.11875	0.1375	0.175	0.1922	0.19375	0.2125	0.25
	11.82								
1000		11.7	11.7	11.7	12.63	11.01	11.7	11.7	11.74
1160		11.82	12.65	12.65	11.71	11.7			
1281.25		11.7	11.7	12.65	11.01	11.7			
1562.5			11.7		12.65				
2125			11.7						
3250			11.7						
4900			11.7						

Table B5: Post-processing Max X-ray Scattering Intensities

Ω/τ (kcal/nm)	Control (no PCND)	0.1	0.11875	0.1375	0.175	0.1922	0.19375	0.2125	0.25
τ (ps)	201.65								
1000		174.97	174.97	174.17	186.31	165.48	174.07	174.64	181.24
1160		203.48	186.27	187.08	174.4	174.59			
1281.25		174.91	175.11	186.09	165.34	173.9			
1562.5			174.29		187.05				
2125			174.2						
3250			174.46						
4900			174.24						

Table B6: Chain Length = 24 beads, Equilibration Times in timesteps

Ω/τ (kcal/nm)	No PCND	0.1	0.11875	0.1375	0.175	0.1922	0.19375
τ (ps)	1586300						
1000		3071800	2371300	4391800	1945300	5143800	654300
1160		2443800	3219800	2143800	5318300	10691800	
1281.25		5000300	2178800	783300	8629800	232800	
1562.5		3313300	4375300	4949300	137300		
2125		3461300	11130300	4398800	155800		
3250		3912800	2549800	885300			
4900		4931800					
5500		5479300					
7750		107300					

Table B7: Chain Length = 24 beads, Pitches in nm

Ω/τ (kcal/nm)	No PCND	0.1	0.11875	0.1375	0.175	0.1922	0.19375
τ (ps)	15.55						
1000		15.63	15.01	15.5	13.64	13.37	13.65
1160		15.05	15.85	15.06	13.22	12.81	
1281.25		15.47	14.15	14.71	13.75	13.29	
1562.5		16.06	15.67	13.77	12.98		
2125		15.87	15.21	13.67	12.79		
3250		13.67	13.29	12.81			
4900		13.79	12.84				
5500		13.79					
7750		12.91					

Table B8: Chain Length = 24 beads, Max X-ray Scattering Intensity

Ω/τ (kcal/nm)	No PCND	0.1	0.11875	0.1375	0.175	0.1922	0.19375
τ (ps)	332.97						
1000		241.68	223.7	212.8	166.48	158.96	130.99
1160		230.29	237.8	216.4	160.58	154.45	
1281.25		231.88	217.43	190.31	170.37	114.57	
1562.5		244.18	220.62	187.13	108.63		
2125		240.14	203.62	180.8	105.18		
3250		191.53	171.22	118.82			
4900		182.73	111.29				
5500		191.8					
7750		119.44					

Table B9: Chain Length = 32 beads, Equilibration Times in timesteps

Ω/τ (kcal/nm)	No PCND	0.1	0.11875	0.1375	0.175
τ (ps)	2078300				
1000		3690300	6231300	4891300	2079800
1160		3690300	2551300	4718300	
1281.25		870300	4419800	4010300	
1562.5		870300	2558800		
2125		1668800			

Table B10: Chain Length = 32 beads, Pitches in nm

Ω/τ (kcal/nm)	No PCND	0.1	0.11875	0.1375	0.175
τ (ps)	18.45				
1000		15.53	17.48	16.09	15.83
1160		16.11	16.59	15.66	
1281.25		16.08	16.15	16.13	
1562.5		16.02	15.44		
2125		15.58			

Table B11: Chain Length = 32 beads, Max X-ray Scattering Intensity

Ω/τ (kcal/nm)	No PCND	0.1	0.11875	0.1375	0.175
τ (ps)	502.18				
1000		247.96	285.49	258.6	207.02
1160		272.9	258.39	254.5	
1281.25		270.9	261.5	240.1	
1562.5		255.1	231.3		
2125		244.4			

Appendix C: Complete Tables of All Defective State Results

Table C1: Simulation Samples for Ω/τ = 0.05 kcal/nm, χN = 55

	τ = 500 ps		τ = 1000 ps		τ = 2125 ps		τ = 3250 ps	
Simulation Number	Equilibrium Alignment Fraction	Annealing Rate (1/ps)	Equilibrium Alignment Fraction	Annealing Rate (1/ps)	Equilibrium Alignment Fraction	Annealing Rate (1/ps)	Equilibrium Alignment Fraction	Annealing Rate (1/ps)
1	0.9045	1.0000E-05	0.9002	1.5385E-05	0.8879	2.5000E-05	0.9016	1.2500E-05
2	0.9136	2.8986E-06	0.9060	1.6667E-05	0.8869	1.8182E-05	0.8839	4.0000E-05
3	0.9080	3.6364E-06	0.9047	3.3333E-05	0.8908	2.5000E-05	0.8824	2.8571E-05
4	0.9079	6.8966E-06	0.9141	4.7619E-06	0.8892	5.0000E-05	0.9175	4.3478E-06
5	0.9093	1.1765E-05	0.9048	2.0000E-05	0.9001	2.2222E-05	0.8738	9.0909E-06
6	0.9109	1.4286E-05	0.9031	4.0000E-05	0.8764	2.0000E-05	0.8822	7.1429E-06
7	0.9053	7.6923E-06	0.8944	1.5385E-05	0.8954	2.8571E-05	0.8756	2.5000E-05
8	0.9115	2.0619E-06	0.8967	7.1429E-06	0.8974	5.0000E-05	0.8900	1.2500E-05
9	0.9185	4.1667E-06	0.9056	3.3333E-05	0.8978	1.5385E-05	0.8978	4.0000E-05
10	0.9107	4.8780E-06	0.8973	1.4286E-05	0.8926	1.3333E-05	0.8831	2.2222E-05
11	0.9026	4.7619E-06	0.8978	4.0000E-05	0.8924	2.2222E-05	0.8950	3.7037E-06
12	0.9104	6.8966E-06	0.9034	2.8571E-05	0.8900	2.2222E-05	0.8809	3.3333E-05
13	0.9084	3.5714E-06	0.9008	1.5385E-05	0.8990	2.2222E-05	0.9055	2.0000E-05
14	0.9063	6.4516E-06	0.8979	1.3333E-05	0.8869	3.3333E-05	0.8793	2.0000E-05
15	0.9157	5.7143E-06	0.9050	5.0000E-05	0.9070	3.3333E-05	0.8713	2.8571E-05
16	0.9126	2.2222E-05	0.9042	3.3333E-05	0.8869	1.3333E-05	0.8924	1.1111E-05
17	0.9103	2.2222E-05	0.8994	4.0000E-05	0.8896	2.8571E-05	0.8827	2.5000E-05
18	0.9192	3.3333E-06	0.9050	1.6667E-05	0.8887	1.6667E-05	0.8986	2.5000E-05
19	0.9016	1.2500E-05	0.9013	2.5000E-05	0.9068	2.8571E-05	0.8979	1.2500E-05
20	0.9037	4.0000E-05	0.8939	6.8966E-06	0.8903	2.5000E-05	0.8763	4.0000E-05
Average	0.9096	9.79772E-06	0.9018	2.3474E-05	0.8926	2.5658E-05	0.8884	2.1030E-05
Standard Deviation	0.0049	9.20136E-06	0.0048	1.3024E-05	0.0072	1.0144E-05	0.0121	1.1757E-05
95% Confidence	0.0023	4.3064E-06	0.0022	6.0954E-06	0.0034	4.7473E-06	0.0057	5.5000E-06

Table C2: Simulation Samples for Ω/τ = 0.1 kcal/nm, χN = 55

	τ = 100 ps		τ = 250 ps		τ = 500 ps		τ = 1000 ps		τ = 2125 ps	
Simulation Number	Equilibrium Alignment Fraction	Annealing Rate (1/ps)	Equilibrium Alignment Fraction	Annealing Rate (1/ps)	Equilibrium Alignment Fraction	Annealing Rate (1/ps)	Equilibrium Alignment Fraction	Annealing Rate (1/ps)	Equilibrium Alignment Fraction	Annealing Rate (1/ps)
1	0.9129	1.7544E-06	0.8937	5.0000E-05	0.8765	2.8571E-05	0.8627	4.0000E-05	0.8460	2.2222E-05
2	0.9107	1.1834E-06	0.8985	1.2500E-05	0.8812	2.8571E-05	0.8719	4.0000E-05	0.8484	2.5000E-05
3	0.9082	2.2989E-06	0.8986	1.5385E-05	0.8761	3.3333E-05	0.8612	5.0000E-05	0.8665	2.8571E-05
4	0.9056	1.2698E-06	0.8946	3.0769E-05	0.8736	4.0000E-05	0.8602	2.2222E-05	0.8340	4.0000E-05
5	0.9105	9.0909E-06	0.8866	8.3333E-06	0.8912	2.5000E-05	0.8761	4.0000E-05	0.8595	6.6667E-05
6	0.9109	1.6064E-06	0.8890	4.0000E-05	0.8729	4.0000E-05	0.8658	2.8571E-05	0.8336	4.0000E-05
7	0.9117	3.1250E-06	0.8825	6.6667E-05	0.8808	5.0000E-05	0.8574	5.0000E-05	0.8609	2.8571E-05
8	0.9063	1.6000E-05	0.8854	6.6667E-05	0.8757	5.0000E-05	0.8764	3.3333E-05	0.8336	5.0000E-05
9	0.9094	1.9048E-06	0.8808	4.4444E-05	0.8589	5.0000E-05	0.8572	3.3333E-05	0.8545	1.3333E-05
10	0.9090	6.2500E-06	0.8959	2.2222E-05	0.8971	2.5000E-05	0.8563	5.0000E-05	0.8354	1.8182E-05
11	0.9076	3.0769E-05	0.8932	2.6667E-05	0.8795	4.0000E-05	0.8568	5.0000E-05	0.8392	5.0000E-05

12	0.9061	5.1948E-06	0.8923	5.0000E-05	0.8818	3.3333E-05	0.8830	1.8182E-05	0.8399	2.8571E-05
13	0.9075	3.2520E-06	0.8968	5.1948E-06	0.8798	2.5000E-05	0.8855	5.0000E-05	0.8424	1.4286E-05
14	0.9104	1.5444E-06	0.8916	5.7143E-05	0.8796	3.3333E-05	0.8503	6.6667E-05	0.8430	3.3333E-05
15	0.9187	1.6393E-06	0.8925	2.8571E-05	0.8827	4.0000E-05	0.8755	1.6667E-05	0.8406	2.8571E-05
16	0.9098	1.3986E-06	0.8934	1.0526E-05	0.8799	2.8571E-05	0.8500	6.6667E-05	0.8411	2.2222E-05
17	0.9066	6.3492E-06	0.8898	4.4444E-05	0.8824	5.0000E-05	0.8527	4.0000E-05	0.8514	2.0000E-05
18	0.9068	2.9630E-06	0.9005	6.6667E-05	0.8780	2.0000E-05	0.8684	4.0000E-05	0.8483	5.0000E-05
19	0.9138	3.3333E-05	0.9020	3.0769E-05	0.8842	1.3333E-05	0.8577	2.0000E-05	0.8491	6.6667E-05
20	0.9084	1.2903E-05	0.8901	5.0000E-05	0.8756	3.3333E-05	0.8616	6.6667E-05	0.8617	5.0000E-05
Average	0.9095	7.1915E-06	0.8924	3.6348E-05	0.8794	3.4369E-05	0.8643	4.1115E-05	0.8465	3.4810E-05
Standard Deviation	0.0031	9.4276E-06	0.0057	2.0183E-05	0.0074	1.0567E-05	0.0106	1.5500E-05	0.0100	1.6150E-05
95% Confidence	0.0015	4.4123E-06	0.0027	9.4461E-06	0.0035	4.9455E-06	0.0049	7.2540E-06	0.0047	7.5586E-06

Table C3: Simulation Samples for $\Omega/\tau = 0.11875$ kcal/nm, $\chi N = 55$

	τ = 100 ps		τ = 250 ps		τ = 500 ps	
Simulation Number	Equilibrium Alignment Fraction	Annealing Rate (1/ps)	Equilibrium Alignment Fraction	Annealing Rate (1/ps)	Equilibrium Alignment Fraction	Annealing Rate (1/ps)
1	0.9001	3.8835E-06	0.8889	2.0000E-05	0.8666	5.7143E-05
2	0.9030	1.8182E-05	0.8853	2.2222E-05	0.8698	3.6364E-05
3	0.9028	2.7586E-06	0.8887	3.0769E-05	0.8861	2.6667E-05
4	0.9029	1.5625E-06	0.8876	5.0000E-05	0.8688	5.7143E-05
5	0.9027	9.3023E-06	0.8781	6.6667E-05	0.8643	5.0000E-05
6	0.9041	8.8889E-06	0.8853	5.0000E-05	0.8702	3.6364E-05
7	0.9076	2.3529E-05	0.8804	2.6667E-05	0.8627	5.0000E-05
8	0.9037	5.3333E-06	0.8907	3.6364E-05	0.8752	3.0769E-05
9	0.9062	4.4444E-05	0.8870	2.2222E-05	0.8734	3.3333E-05
10	0.9009	1.9048E-05	0.8905	3.3333E-05	0.8722	4.0000E-05
11	0.9075	1.9048E-05	0.8838	5.7143E-05	0.8742	3.6364E-05
12	0.9028	2.0833E-06	0.8742	3.3333E-05	0.8728	3.0769E-05
13			0.8875	4.0000E-05	0.8861	2.3529E-05
14			0.8988	1.6000E-05	0.8703	5.7143E-05
15			0.8844	5.7143E-05	0.8533	3.3333E-05
16			0.8864	4.0000E-05	0.8712	5.0000E-05
17			0.8920	6.6667E-05	0.8559	8.0000E-05
18			0.8895	2.8571E-05	0.8786	5.7143E-05
19			0.8821	4.0000E-05	0.8664	5.0000E-05
20					0.8621	5.0000E-05
Average	0.9037	1.3172E-05	0.8864	3.8795E-05	0.8700	4.4303E-05
Standard Deviation	0.0023	1.2529E-05	0.0054	1.5431E-05	0.0083	1.3866E-05

95% Confidence	0.0015	7.9602E-06	0.0026	7.4376E-06	0.0039	6.4896E-06

Table C4: Simulation Samples for Ω/τ = 0.1375 kcal/nm, χN = 55

	τ = 100 ps		τ = 250 ps		τ = 500 ps	
Simulation Number	Equilibrium Alignment Fraction	Annealing Rate (1/ps)	Equilibrium Alignment Fraction	Annealing Rate (1/ps)	Equilibrium Alignment Fraction	Annealing Rate (1/ps)
1	0.9004	5.3333E-06	0.8779	2.5000E-05	0.8656	8.0000E-05
2	0.9007	3.8835E-06	0.8753	6.6667E-05	0.8524	8.0000E-05
3	0.8969	4.5977E-06	0.8722	1.0000E-04	0.8607	6.6667E-05
4	0.9001	8.8889E-06	0.8846	3.6364E-05	0.8686	4.4444E-05
5	0.8992	8.0000E-06	0.8753	5.0000E-05	0.8563	8.0000E-05
6	0.9228	3.5714E-06	0.8720	1.0000E-04	0.8680	6.6667E-05
7	0.9108	7.8431E-06	0.8712	5.7143E-05	0.8552	1.3333E-04
8	0.9046	3.5088E-06	0.8909	6.6667E-05	0.8545	5.7143E-05
9	0.8969	1.0256E-05	0.8799	4.4444E-05	0.8577	8.0000E-05
10	0.8975	5.7971E-06	0.8764	6.6667E-05	0.8537	5.7143E-05
11	0.9013	4.4444E-05	0.8742	2.1053E-05	0.8532	6.6667E-05
12	0.8942	7.0175E-06	0.8805	6.6667E-05	0.8644	3.6364E-05
13	0.9044	3.3333E-05	0.8782	1.0000E-04	0.8552	5.0000E-05
14	0.8986	1.0000E-05	0.8803	4.4444E-05	0.8674	5.0000E-05
15	0.9075	1.0526E-05	0.8769	6.6667E-05	0.8650	6.6667E-05
16	0.8921	3.6364E-05	0.8702	5.7143E-05	0.8512	5.0000E-05
17	0.9007	7.1429E-06	0.8777	5.7143E-05	0.8633	5.0000E-05
18			0.8920	6.6667E-05	0.8587	8.0000E-05
19			0.8716	4.0000E-05	0.8689	3.6364E-05
20			0.8708	4.4444E-05	0.8590	5.0000E-05
Average	0.9017	1.2383E-05	0.8774	5.8859E-05	0.8600	6.4073E-05
Standard Deviation	0.0071	1.2615E-05	0.0061	2.2468E-05	0.0060	2.1884E-05
95% Confidence	0.0033	5.9040E-06	0.0029	1.0515E-05	0.0028	1.0242E-05

Table C5: Simulation Samples for Ω/τ = 0.05 kcal/nm, χN = 41.5

	τ = 100 ps	
Simulation Number	Equilibrium Alignment Fraction	Annealing Rate (1/ps)
1	0.9024	8.1633E-06
2	0.8976	6.3492E-06
3	0.9250	7.3665E-07
4	0.8976	1.5267E-06
5	0.9049	6.2500E-06
6	0.9072	1.3158E-06
7	0.8986	7.0299E-07
8	0.9042	2.6667E-06

9	0.9000	5.8824E-06
10	0.8929	7.7973E-07
11	0.8977	7.2727E-06
12	0.9013	8.1301E-07
13	0.9043	2.5000E-05
Average	0.9026	5.1892E-06
Standard Deviation	0.0078	6.5950E-06
95% Confidence	0.0036	3.0866E-06

Table C6: Simulation Samples for Ω/τ = 0.1 kcal/nm, χN = 27

	τ = 100 ps
Simulation Number	Equilibrium Alignment Fraction
1	0.5786
2	0.4497
3	0.5842
4	0.4924
5	0.5795
6	0.5713
7	0.4372
8	0.4388
9	0.4850
10	0.5819
11	0.5704
12	0.5692
13	0.4437
14	0.5749
15	0.5695
16	0.5264
Average	0.5283
Standard Deviation	0.0595
95% Confidence	0.0279

References:

1: Lawson, Richard A. Peters, Andrew J. Ludovice, Peter J. Henderson, Clifford L. "Coarse Grained Molecular Dynamics Model of Block Copolymer Directed Self-Assembly" Proc. SPIE 8680, Alternative Lithographic Technologies V, 86801Y (April 5, 2013); doi:10.1117/12.2021439.

2: Langer, Karol M. Sevink, G. J. A. "Mesoscale Modeling of Block Copolymer Nanocomposites," Soft Matter, 21 October 2014, Issue 39, Page 7671 to 7898.

3: Xu, Weiquan. Zhang, Pingwen. "Boundary effects in confined copolymer system and compressible SCFT model." Journal of Computational and Applied Mathematics 265 (2014) 290–300.

4: Fried, H. Binder, K. "The microphase separation transition in symmetric diblock copolymer melts: A Monte Carlo study" The Journal of Chemical Physics 94 , 8349 (1991); doi: 10.1063/1.460067

5: Jenkins, Jerry W. "Novel Efficient Simulation Techniques for Use in Molecular Modeling". Published by Georgia Institute of Technology, July 2000. Retrieved from Smartech at the Georgia Tech Library. URL: https://smartech.gatech.edu/handle/1853/11238

6: Hanggi, P.; Mroczkowski, T. J.; Moss, F.; McClintock, P. V. E. "Bistability driven by colored noise: Theory and experiment"; *Physical Review A*. (1985), 32: p. 695.

7: Yager, Kevin G. Lai, Erica. Black, Charles T. "Self-Assembled Phases of Block Copolymer Blend Thin Films" American Chemical Society, Oct 6 2014, p. 10582–10588

8: Xu, Ting. Kim, Ho-Cheol. Deouchey, Jason. Seney, Chevey. Levesque, Catherine. Martin, Paul. Stafford, C.M. Russel, T.P. "The influence of molecular weight on nanoporous polymer films." Polymer (2001) Apr 3 2001.

9: Zhao, Xinyu. Lee, Soo-Young. Choi, Jin. Lee, Sang-Hee. Shin, In-Kyun. Jeon, Chan-Uk. "Minimization of

line edge roughness and critical dimension error in electron-beam lithography" Journal of Vacuum Science & Technology B 32 , 06F505 (2014); doi: 10.1116/1.4899238

10: Langeloth, Michael. Masubuchi, Yuichi. Böhm , Michael C. Müller-Plathe, Florian. "Reptation and constraint release dynamics in bidisperse polymer melts" The Journal of Chemical Physics 141 , 194904 (2014); doi: 10.1063/1.4901425

11: Doi, M. Graessley, W. W. Helfand, E. Pearson, D. S."Dynamics of polymers in polydisperse melts" Macromolecules 1987 20 (8), 1900-1906

12: Kornreich, M. Avinery, R. Beck, R. "Modern X-ray scattering studies of complex biological systems" Current Opinion in Biotechnology. 2013, 24:716–723

13: Nozue, Yoshinobu. Shinohara, Yuya. Ameniya, Yoshiyuki. "Application of Microbeam Small- and Wide-angle X-ray Scattering to Polymeric Material Characterization", 2007, Polymer Journal, Vol. 39, No. 12, pp. 1221–1237

14: Stribek, Norbert. "X-ray Scattering of Soft Matter" Springer Laboratory Manuals in Polymer Science. ISBN: 3-540-46488-4